1-1-2005

Guarded hot plate apparatus design and construction for thermal conductivity measurements

Dave Reid
Ryerson University

GUARDED HOT PLATE APPARATUS DESIGN AND CONSTRUCTION FOR THERMAL CONDUCTIVITY MEASUREMENTS

by

Dave Reid

B.Eng. University of Technology,
Jamaica 1996

A thesis presented to

Ryerson University

in partial fulfillment of the
requirements for the degree of
Master of Applied Science

in the Program of
Mechanical Engineering

Toronto, Ontario, Canada, 2005

AUTHOR'S DECLARATION

I hereby declare that I am the sole author of this thesis.

I authorize Ryerson University to lend this thesis to other institutions or individuals for the purpose of scholarly research.

_____

I further authorize Ryerson University to reproduce this thesis by photocopying or by other means, in total or in part, at the request of other institutions or individuals for the purpose of scholarly research.

_____

ABSTRACT

GUARDED HOT PLATE APPARATUS DESIGN AND CONSTRUCTION FOR SOIL THERMAL CONDUCTIVITY MEASUREMENTS

Dave Reid

Master of Applied Science, 2005
Program of Mechanical Engineering, Ryerson University

A Guarded Hot Plate (GHP) apparatus was designed and built for high temperature applications, consistent with or better than the established standards. This apparatus consists of a hot and a cold plate, attached to a frame, which allows the plates to be tilted from horizontal to vertical and configured for heating from the top to the bottom. The plates are independently heated by passing heat transfer fluid through a flow distribution system consisting of manifolds and internal flow passages, machined in each plate. Attached to the hot plate are an electrically heated heater plate and a heat flux meter, configured consistent with the hybrid method for measuring heat flux.

This apparatus is designed to measure thermal conductivity of soils at different moisture contents and for temperatures ranging from -20°C to 200°C. An error analysis for the thermal conductivity measurement shows a conservative estimate of the bias error to be around ± 2%.

ACKNOWLEDGEMENTS

The author would like to acknowledge Dr. W. Leong for his invaluable advice and guidance throughout the project.

The author would like to acknowledge the support of Petro-Canada Limited for the in-kind contribution of heat transfer fluid, Calflo LT, and Connect Tech Inc. for the in-kind contribution of a Blue-heat PCI card, which are invaluable to this project.

The author is most grateful to the Ryerson Mechanical Engineering Support staff especially Joseph Amankrah, Andrew Heim and Alan Machin, for their time and assistance through the building and set-up phases of the experiment.

Last, but by no means least, the author would like to thank his family and friends for their endless support and encouragements.

TABLE OF CONTENT

List of Figures

List of Tables

Nomenclature

A	Cross-sectional area [m^2]
B	Bias error
C	Turning loss coefficient
D	Diameter [m]
e	Heat flux meter *emf* output [mV]
f	Moody's coefficient of friction
GHP	Guarded Hot Plate
H	Flow resistance
HFM	Heat flux meter
h	Heat transfer coefficient [W/m^2K]
K	Loss coefficient
L	Length [m]
l	Depth of hole [m]
N	Number of
P	Pressure [N/m^2]
P′	Electrical Power [W]
Q	Dimensionless flow rate
q''	Heat flux [W/m^2]
q	Heat transfer rate [W]
RTD	Resistance temperature detector
S	Standard error (or precision index)
T	Temperature [K]
t	Time [s]
t′	Student's t multiplier
U	Overall uncertainty
V	Velocity [m/s^2]

Greek

α	Proportional constant for HFM [W/mV]
β	Bias error
σ	Standard deviation
δT	Small temperature difference [K]
ΔT	Temperature difference between hot and cold plates [K]
Δx	Thickness [mm]
ε	Precision error
ω	Resistance coefficient [m^{-1}]
λ	Thermal conductivity [W/mK]
ξ	Fractional wire perimeter

ρ	Density [kg/m^3]
θ	Sensitivity coefficient
υ	Degrees of freedom

Subscripts

a	Ambience
b	"Back" heat transfer rate
c	Cold plate
e	Heater plate electrical power
h	Hot plate
htr	Heater plate
m	Mean value
md	Between wire and medium
s	On the surface
sa	Between wire and ambience
smd	Between wire and medium on the surface

CHAPTER 1

THERMAL CONDUCTIVITY MEASUREMENT OF SOILS

1.1 Introduction

The prediction, or accurate determination, of the effective thermal conductivity λ of soil is very important in many heat and mass transfer phenomena. The heat flow through soil is controlled by its effective thermal conductivity and by temperature gradients. Heat flow problems in soil are of interest to scientists concerned with the temperature distribution in the soil, the energy balance at the soil surface, the artificial heating of soil for enhanced crop production and soil behavior under conditions of forest fire. Also, engineers are interested in geothermal energy extraction and heat flow away from industrial installation in the ground such as underground high-voltage cables, ground heat pumps and heat exchangers, cross-country oil pipelines and buildings.

The effective thermal conductivity of soil is a function of a wide variety of properties related to the classification of soil, including the mineral composition of the solid particles, texture, pore size distribution and porosity. External factors of the soil also affecting its effective thermal conductivity include dry density, temperature and water content of the medium. Heat flow occurs by conduction through the soil particles, through the water present as continuous films on the particles, or as annuli at the point of contact between particles and through the air in the soil pores, if the soil is not fully saturated. Heat transfer in moist soil also occurs as a result of vapor diffusion. Water vapor

molecules diffuse from warm regions where evaporation occurs to cold regions where condensation occurs as a result of vapor pressure gradients caused by temperature differences.

As a result of the growing demand for accurate soil effective thermal conductivity measurements, there is a variety of absolute or comparative methods currently available. These methods of thermal conductivity measurements include both transient, such as hot wire, laser flash and heated probe, and steady state, namely guarded hot plate (GHP), techniques. The transient technique is widely used because it utilizes smaller specimen sizes. The equipment used is portable, which makes them very convenient. The transient technique will produce quick and easy measurements, which make this method most suitable for field applications. A disadvantage of the transient technique for thermal conductivity measurements of soil is questionable measurement results. Localized drying around the needle or wire, as well as air gaps, can introduce large errors in some forms of this technique. While the need for soil specimen heat capacity and density to be known accurately is important to obtaining reliable data in others.

Steady state techniques (either absolute or comparative) are also used to measure thermal conductivity. These techniques operate on a simple theory, which requires carefully monitored heat input, accurate temperature measurement and a well controlled pattern of heat flow. Even though these techniques demand great care in experiments that are time consuming, they are the benchmark by which simple and rapid transient techniques as well as industrial measurements are assessed. For these reasons, this research was conducted to design and build a single specimen GHP apparatus.

1.1.1 The Guarded Hot Plate Method

The guarded hot plate method is a steady state technique. The basic principle of this method is to generate a steady and known heat flux in a metering device to flow unidirectionally through the specimen so that it appears as a slab of infinite width bounded by parallel planes. A hot plate consisting of two parts, a heater plate (or metering area) surrounded by an annular guard, in the form of the main plate (shown in Figure 1-1), is commonly used to supply the required heat flux. The hot and heater plates are separated by a small air gap, which acts as a thermal barrier. The cold plate is maintained at a stable lower temperature, constant to within a few hundredths of a degree Celsius, to accommodate the heat flows from the metering area of the hot plate through the specimen.

The hot plate is heated independently of the metering area heater plate, which is usually electrically heated. The heat flux produced serves to maintain the heat flow perpendicular to the hot face in the central metering region, thereby creating isothermal planes across the measured region of the specimen. The effective heater plate area, and thus the area of the specimen, is defined as the area contained within a line drawn mid-way between the gap separating the guard and metering area heaters. Heat transfer across the gap via the specimen can be reduced either by making the specimen the same size as the metering area, thus filling the guard area with relatively low conductivity insulation, or making the metering and guard areas of equal temperature.

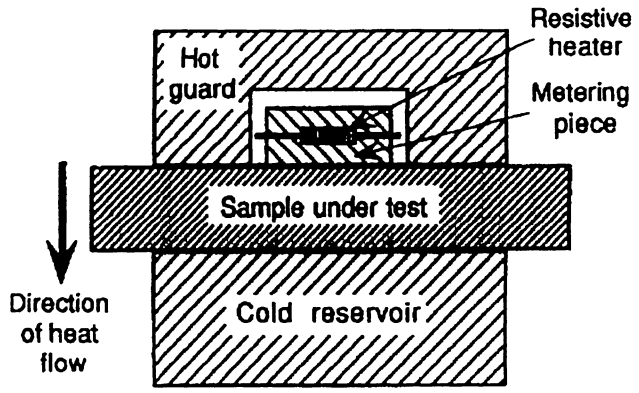

Figure 1-1 Sketch of a single specimen GHP apparatus (Dey *et al.* [1]).

1.1.2 Scope of Research

The objective of this research was to design and build a guarded hot plate apparatus. This apparatus would allow the performance of thermal conductivity analysis for several classifications of soils at different moisture contents (from dry to saturated) over a wide range of temperatures, ranging from -20°C to 200°C, so as to provide a complete range of data, which could be incorporated into soil effective thermal conductivity models that can be universally tested, verified and further improved if necessary. Once the thermal conductivity model is validated, it can be programmed into simulation software for such applications as ground thermal storage and heat and moisture transfer around earth-bound structures. This thermal conductivity analysis can be derived by a steady state method, which is more accurate and gives reliable data; thus, a GHP apparatus was designed and built for high temperature applications.

The construction of this GHP apparatus took place after a detailed design analysis was done for materials most suited to minimize errors. The plate's materials were chosen for their ability to give uniform temperature distributions across their surfaces while minimizing the temperature variations

during experiments. All the components used in the construction of this equipment exceeded the high temperature demand of the apparatus. The design of the apparatus was consistent with or better than the established standards, such as the ISO International Standard: Thermal Insulation - Determination of Steady-State Thermal Resistance and Related Thermal Insulation - Determination of Steady-State Thermal Resistance and Related Properties - Guarded-Hot-Plate Apparatus (ISO 8302) and ASTM Test Method for Steady-State Heat Flux Measurements and Thermal Transmission Properties by Means of the Guarded-Hot-Plate Apparatus (C 177). Analysis shows a conservative estimate of the bias error for the thermal conductivity measurement to be around ± 2 % at the high temperature of 200°C and large temperature difference of 10°C between the hot and cold plates (see Chapter 6).

1.2 Literature Review

Of the comprehensive literature available on the theoretical modeling of soil thermal conductivity, such as Gori and Corasaniti [2], Tarnawski and Leong [3], Tarnawski and Gori [4], Shiozawa and Campbell [5], none has been verified extensively against experimental data at high temperatures. At most, the data available to verify these predictions are at low and moderate temperatures ($T < 70°C$), such as Sepaskhah and Boersma [6], Campbell *et al.* [7], Hiraiwa and Kasubuchi [8], among others. Due to the lack of credible data, the results of soil thermal conductivity predicted at high temperature vary considerably. Of these few papers dealing with high temperature thermal conductivity measurements, most lack satisfactory information about soil texture and mineralogical composition, as well as exhibit questionable accuracy. Also, experiments are done over limited ranges of temperature and the classification of soil is not widely available. Despite these limitations, these published data are used extensively in theoretical models and simulation software for comparative purposes.

Experimental thermal conductivity data, for three soil types, loamy sand, loam, and silty clay loam, were published by Sepaskhah and Boersma [6], measured by a heated probe at temperatures of 25°C and 45°C. The soil specimens were air dried and packed in a glass jar. Each specimen contained equal numbers of dried soil scooped in the jar, which was tapped on the bench after each scoop was added. For the desired moisture contents, water was added to the soil in the jar or sprinkled onto evenly spread soil on a plastic sheet then mixed in a plastic bag. The containers were then capped with a lid and sealed with tape before being placed in a constant temperature cabinet for several weeks, to ensure uniform water distribution. There are, however, some problems with the soil texture, porosity, and bulk density data provided. It appears that porosity data for the loamy sand was misprinted. Also, for the other two soils, the given dry bulk density and porosity data give an unusually high density of solids.

Comprehensive thermal conductivity data sets at high temperature for nine soils, belonging to three textural groups, were published by Campbell *et al.* [7]. The samples can be classified as, coarse soils: L-soil, Royal, Volkmar; medium soils: Palouse-A, Salkum, Mokins, Walla Walla; and fine soils: Palouse-B, Bouldercreek. Samples were air-dried and passed through a 2-mm sieve, before being moistened to a pre-determined moisture content, mixed and packed to a uniform bulk density in a pipe. The plastic pipe used was covered and tape sealed, then stored in a controlled temperature oven prior to measurement. A heated probe, 0.9 mm diameter and 40 mm long, was used to measure thermal conductivity in the range from 30°C to 90°C at 20°C intervals. The soil data, however, lacks certain information, such as the mineralogical composition and grain size distribution for some soils. Consistent data were obtained at 30°C and 50°C, over the range of moisture content. While at higher temperatures (70°C and 90°C), the data were sporadic and show random thermal conductivity variation with respect to moisture content.

Hiraiwa and Kasubuchi [8] published thermal conductivity data for two soils, Red Yellow soil and Ando soil, exposed to temperatures ranging from 5°C to 75°C, at 10°C intervals. Again, samples were air-dried and passed through a 2-mm sieve, before been moistened to a pre-determined moisture content, by either adding water and mixing in a plastic bag before packing in a sampler, or by packing dried soil in a sampler, adding water then repeatedly being heated in a microwave oven, then cooled several times. The sampler was capped with a hard plastic lid and sealed with a silicon sealant and placed in a constant temperature box, controlled to ± 0.01°C. Moisture content of soil samples was evenly spread over the range of wetness, from dry to fully saturated. Twin heat probes made of stainless-steel needles, 50 mm long with outer and inner diameters of 1 mm and 0.5 mm, respectively, measured the thermal conductivity. The measurements were repeated several times for the same soil sample to determine an averaged thermal conductivity value.

Thermal conductivity measurements, published by Black *et al.* [9] were done using samples of Ottawa sand with both heated probes and a GHP apparatus. However, the temperature range over which the measurements were made was not included in the literature. The correlated data for thermal conductivity for the range of moisture content measured is poorest at low moisture content; this is attributed mainly to moisture migration around the probes. As a result, the thermal conductivity measurement, on average, is lower for the heated probe than for the GHP apparatus.

1.2.1 Observations

As a result of the growing demand for accurate soil effective thermal conductivity measurements, there are a variety of absolute and comparative methods currently being used. However, the steady state technique of the GHP apparatus will provide more accurate experimental data than the popular heated probe, as confirmed by earlier publications. With a complete range of data, for temperatures

from -20°C to 200°C and moisture content from dry to saturated, a soil effective thermal conductivity model can be developed that should be universally tested, verified and further improved if necessary. Therefore, the use of the GHP apparatus rather than more traditional methods will provide superior accuracy in experimental data for readily available and widely used soils, such as Ottawa sand, which are used extensively in theoretical models and simulation software.

CHAPTER 2

THEORETICAL CONSIDERATION OF GHP

2.1 History of GHP

The thermal conductivity measurement of poor conductors, such as building insulation material, by the Guarded Hot Plate (GHP) technique has been in existence, in various forms, since the late 1890's, whereas similar measurements on metals dated back to at least the late 18th century (Salmon [10]). The earliest known quantitative work done with the guarded hot plate technique was in 1898 by Lees, of England (Zarr [11]). He used a pair of specimens clamped between three copper plates. The central plate was electrically heated by applying a known amount of electrical power, thus allowing the heat to flow axially through the specimens to the outer plates, which were kept at a slightly lower temperature. The surface temperatures of the two specimens, measured with thermocouples, were assumed to be the same as those of the adjacent copper plates. The thermal conductivity, λ, of the specimen was deduced by a form of the Fourier Equation for heat conduction in one dimension:

$$\lambda = \frac{q\Delta x}{A(T_h - T_c)} \qquad (2.1)$$

Here, the heat transfer rate q, which is equal to one half (1/2) the power supplied to the central plate, assuming the heat flux is shared equally between the two specimens, (T_h-T_c) is the mean temperature difference between the central and outer plates, A and Δx are the cross-sectional area of the central plate and the mean thickness of the specimen, respectively.

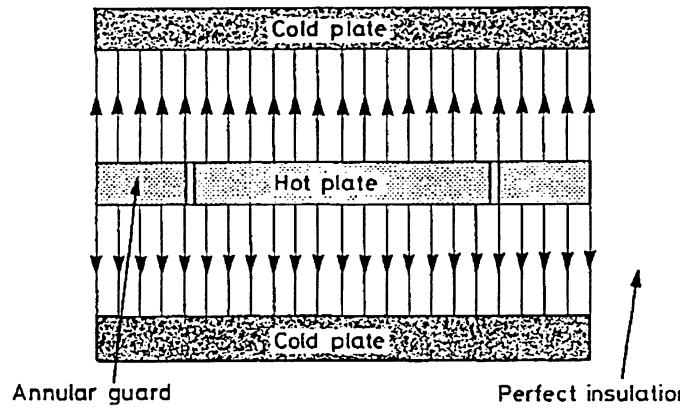

Figure 2-1 Outline of a GHP apparatus (Salmon [10]).

Peonsgen modified the guarded hot plate apparatus in 1910 in Germany. An annular copper guard was introduced around the heater plate, as shown in Figure 2-1, and this guard is maintained isothermal to the heater plate in order to minimize radial heat loss. Annular shields were also used between the guards and the cooled plates around the specimens; these shields were made of relatively low conductivity material such as cork dust. The low conductivity shields provide additional guard to the specimens, thus minimizing edge heat loss, as illustrated in Figure 2-2. These modifications provide for better linear heat flow in the axial direction, thus allowing more reliable measurements to be recorded generally over the earlier design, as well as for thicker specimens.

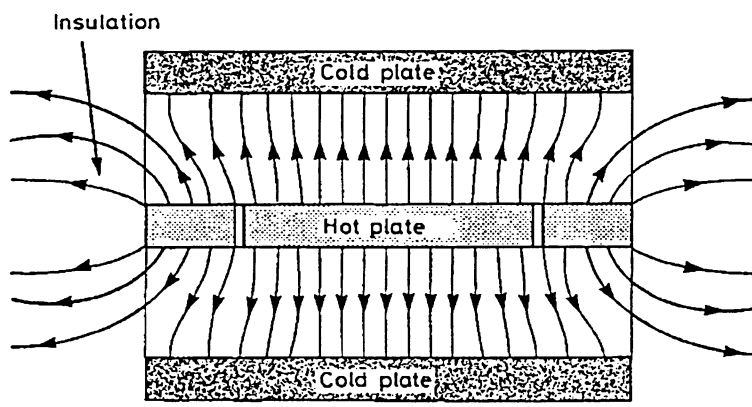

Figure 2-2 Practical sketch of a GHP apparatus (Salmon [10]).

Once again, in Germany, Jakob provided further modification to the existing design resulting in an apparatus which requires a single specimen, similar in design to the apparatus shown in Figure 1-1. An auxiliary guard plate maintained at the same temperature as the heater plate was added to the back surface of the heater plate separated by a layer of insulation, essentially constraining heat flow to only one direction, through the single specimen. The thermal conductivity measured using this design conforms to the same fundamental equation, Eq. (2.1), except that the values are no longer mean values and q is the power supplied to the heater plate. This technique has since become well established and recognized as the most accurate technique for measuring thermal conductivity of poor conductors and as such it is documented in several written standards such as the ISO International Standard (C 177).

2.2 The Thermal Conductivity Measurement Strategy

The thermal conductivity derivation is based on Fourier's Law, which is given by Eq. (2.2)

$$q'' = \lambda\left(\frac{\Delta T}{\Delta x}\right) \tag{2.2}$$

Here, λ is the thermal conductivity of interest, q'' is the heat flux through the specimen, ΔT and Δx are the temperature difference and distance across the specimen. The heat flux can be measured directly and precisely using a technique called the hybrid method, as documented by Hollands [12]. This method constitutes a primary measurement method, which traces back to the first law of thermodynamics, and a secondary method, which uses a form of Newton's law of cooling. A configuration realizing a hybrid method is shown in Figure 2-3. The heat transfer rate on a hot

surface of interest q is measured with a combination of three components: an electrically-heated heater plate; a thermopile heat flux meter; and a temperature-controlled isothermal hot plate, which has a recess cut into it to contain the heater plate and the heat flux meter. The heat flux meter, whose *emf* output is a very sensitive measure of (and proportional to) the temperature difference across it, is sandwiched between the heater plate and the hot plate. This combination of heater plate and heat flux meter can be used to measure the heat transfer as follows. A steady state heat balance of the heater plate gives

$$q = q_e - q_b \tag{2.3}$$

where q is the heat transfer rate of interest, *i.e.,* the heat going into the soil sample, q_e is the electrical power input to the heater plate (equal to the product of the voltage and current of the electrical resistance inside the heater plate, *i e.,* $q_e = VI$); and q_b is the "back" heat transfer rate passing to the hot plate, mainly through the heat flux meter. The heat flow rate q_b is equal to αe, where α is a proportionality constant derived by calibration (Appendix A), and e *is* the *emf* output of the heat flux meter. Note that this equality is a form of Newton's law of cooling, where $e \propto \delta T$ which is the temperature difference between the heater plate and the hot plate. It should be noted that q_b includes heat transfer over the *entire* back surface of the plate, as well as through electrical wires and support bolts securing the heater plate in its location. On the other hand, because the heater plate and the hot plate are both isothermal but of differing temperatures, the *emf* output e of the heat flux meter is proportional to the heat flow rate q_b, even though the heat flux meter touches only part of the back surface of the heater plate. Thus, the proportionality of q_b to e will remain, provided the other ends of the electrical wires and the support bolts are heat sinked to the hot plate. The calibration to determine the proportional constant α of the heat flux meter was done *in situ* after assembly of the entire apparatus (see Appendix A).

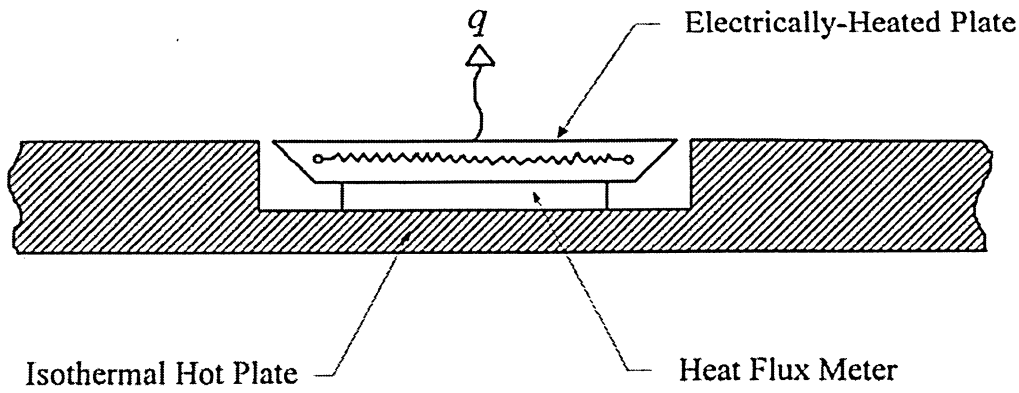

Figure 2-3 The hybrid configuration for heat transfer measurement (Leong [13]).

2.3 Standards and Expectations

A number of measures must be taken in order to obtain ideal or near adequate conditions. Highly conducting material must be used to make the plates of the apparatus to achieve uniformity of temperature across their surfaces, which must be as flat as possible. Along with the aforementioned properties, when measuring low-density insulations, the plates should have high emissivity surfaces, since radiative heat transfer is an important component of the apparent thermal conductivity. In order to maintain unidirectional heat flow across the specimen, the temperature balance between the guard and the metering area must also be maintained within close limits (0.01°C), thus preventing lateral heat exchange. For effective shielding of the heater plate, the width of the annular guard should be at least one quarter the width of the metering area and not less than the thickness of the specimen. The contact resistance between the plates and the specimen should be as uniform as possible over the whole surface to ensure there is uniform heat flow into the specimen.

For accurate temperature measurement, the temperature sensors (thermocouples and RTDs) mounted in the hot and cold plates must be in good thermal contact with the plates themselves. They must be properly calibrated to read the required temperature or the temperature difference between the plates.

The thermocouples and RTDs should be in good contact with and preferably mounted on the specimen surfaces for materials with thermal conductivities greater than about 0.15 W/mK [10]. The wires of the thermocouples and RTDs mounted on the plate's surfaces must run in an isothermal region, to limit heat flow along them. This would reduce the error in the temperature being measured and thus ensure that the thermocouples indicate the correct plate temperature. To limit the magnitude of such errors, the thermocouples should be made from fine wire (0.2 mm thick or less), and their thermal contact resistance with the plates/specimens should be reduced using a contact medium such as zinc oxide, suitable cement or epoxy. The heat flow between the edges of the specimens and the apparatus plates can be controlled with adequate insulation; this is particularly important both for materials of low thermal conductivity and for thick specimens.

CHAPTER 3

APPARATUS DESIGN AND CONSTRUCTION

3.1 Overview of Apparatus

A sketch of a single specimen guarded hot plate apparatus shown in Figure 3-1 was designed for high temperature thermal conductivity measurement of soil samples. The apparatus was designed to operate through a range of temperatures from -20°C to 200°C for varying specimen thickness up to 38.1 mm (1 ½ in.). This model consists of hot and cold plates attached to a self-leveling frame (not shown), which allows the frame supports to be pivoted through various angles from horizontal to vertical, as well as configured for heating from the top or the bottom. The plates are independently heated by the passing of a stream of heat transfer fluid through a series of passages drilled in each plate, which is fitted with three manifolds. Attached to the hot plate are an electrically heated heater plate and a heat flux meter, configured consistent with the hybrid method.

Isothermal condition of the heater plate and the hot plate is needed to make the hybrid method work well. Both of the surfaces must be isothermal for a single δT to apply, and the surfaces would be isothermal if the plates are isothermal. Hence, to achieve an isothermal condition, or at least only very modest temperature variations inside the plates, the plates were made of a good conductor. Except for the heat flux meter, the entire hot plate apparatus is made of 99.8 percent pure copper, which has a high thermal conductivity, is relatively easy to machine, and can be soldered together

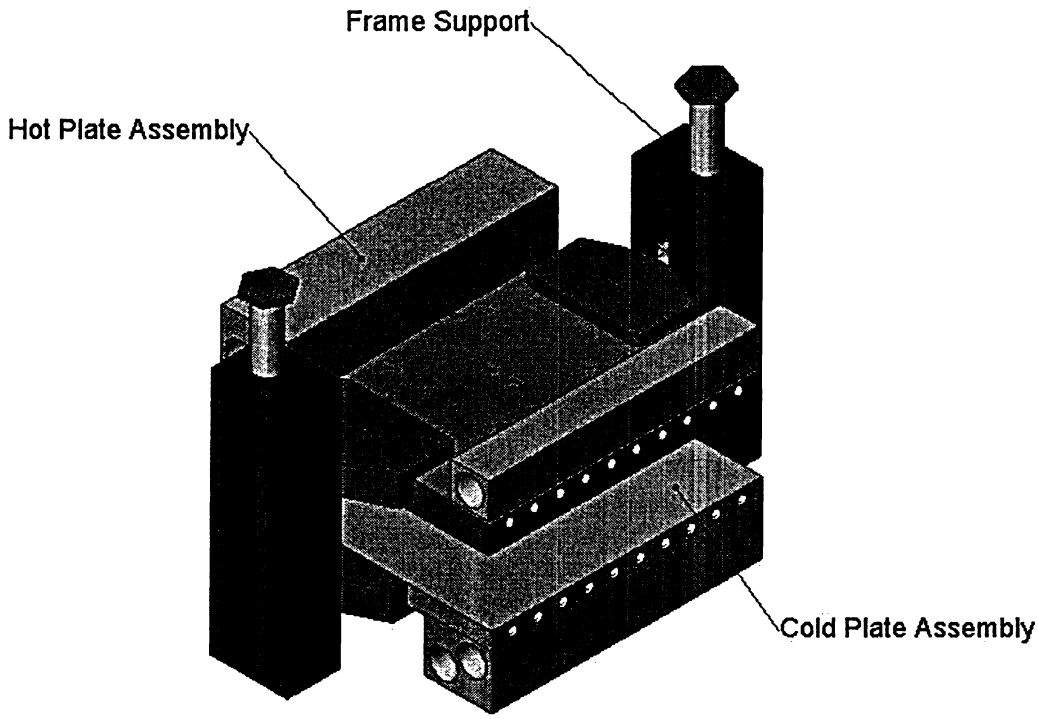

Figure 3-1 3-D sketch of single specimen GHP apparatus.

with little thermal contact resistance; thus, each heated plate (namely hot plate, cold plate, and heater plate) would have a uniform temperature, despite the strong variation of heat flux over the plate (see Chapter 4). These plates, as well as all other components used in this apparatus, are all rated at high temperatures and as such are chosen because of their ability to satisfy these demands on the apparatus.

Two thermally controlled circulating baths are used to maintain the temperatures of the hot plate and the cold plate, by passing a stream of heat transfer fluid, Calflo LT, from each bath through inlet, crossover and outlet manifolds soldered to each plate, as sketched in Figure 3-2. Thermocouple junctions embedded inside the hot and cold plates are connected in series to form a thermopile, which measures the temperature difference between the plates' surfaces. Embedded Platinum Resistance Temperature Detectors (RTDs) measure the plates' surface temperatures. The apparatus is designed

in such a way that the temperatures of the heater plate and the hot plate are made equal by adjusting the electrical power to the heater plate until the *emf* output of the heat flux meter becomes essentially zero. When the apparatus is at steady state, data acquisition can begin. In this case, the electrical power q_e is equal to the heat transfer of interest q, because the back heat transfer q_b is negligibly small.

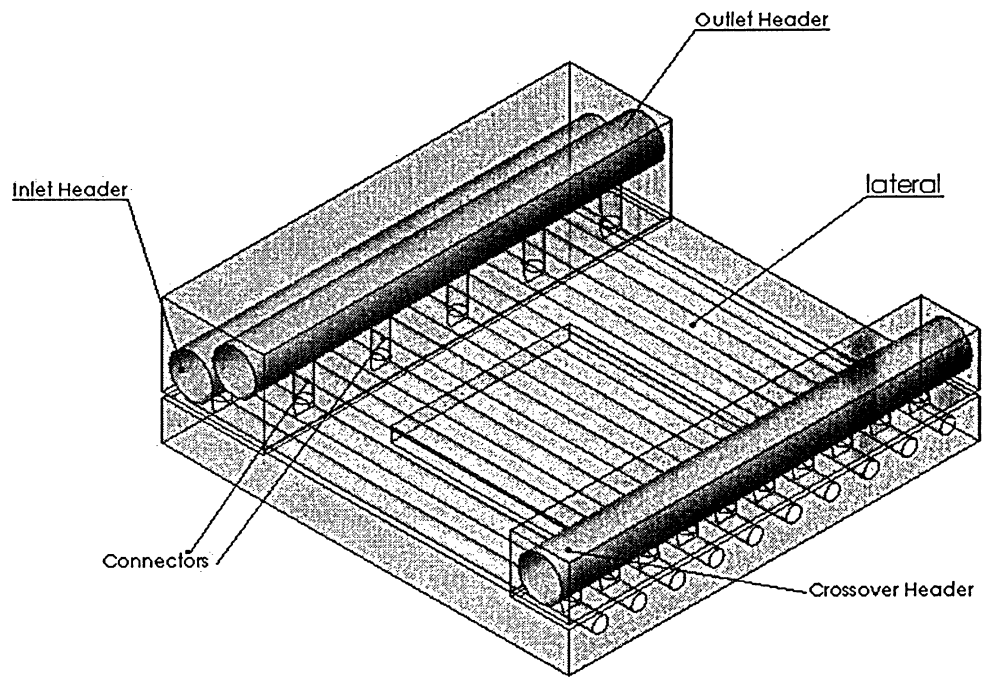

Figure 3-2 Internal flow passage of the hot plate with three manifolds.

3.2 The Hot and Cold Plates

To minimize temperature variation during experiments, and also to have good machining properties, the plates were made from a material with a very high thermal conductivity; hence, the

plates are made of copper. The hot plate dimensions are 177.8 × 177.8 mm and 19.05 mm thick with inlet/outlet and crossover headers for the ten internal flow passages. To contain the HFM and the heater plate, a recess 77.8 × 77.8 mm and 6.35 mm deep was machined in the center of the hot plate. Similarly, another copper plate, 12.7 mm thick, was used to make the cold plate, which is also drilled with ten internal flow passages. A total of eight through holes were carefully drilled through the recess for passing the fastening bolts, wires of the heater plate, and wires of the HFM out to the back of the hot plate, as shown in Figure 3-3. The flatness tolerance of ±0.05 mm for the front surfaces of the plates were maintained and checked after machining work was done. Six holes with 3.18 mm diameter were drilled to within 1.59 mm from the front surface of each of the hot and cold plates. Four holes with 17.46 mm in depth and two holes (positioned near the center of the hot plate over the existing recess) 11.11 mm in depth were drilled at the back of the hot plate for embedding temperature sensors; similarly, six 11.11 mm deep holes were drilled at the back of the cold plate. The dimensions of the holes were designed according to Beck and Hurwicz [14] and Moffat [15] to minimize the error in the thermocouple measurements of the undisturbed surface temperatures of the plates. Appendix D provides the detail engineering drawings and dimensions of the plates and other components of the GHP apparatus.

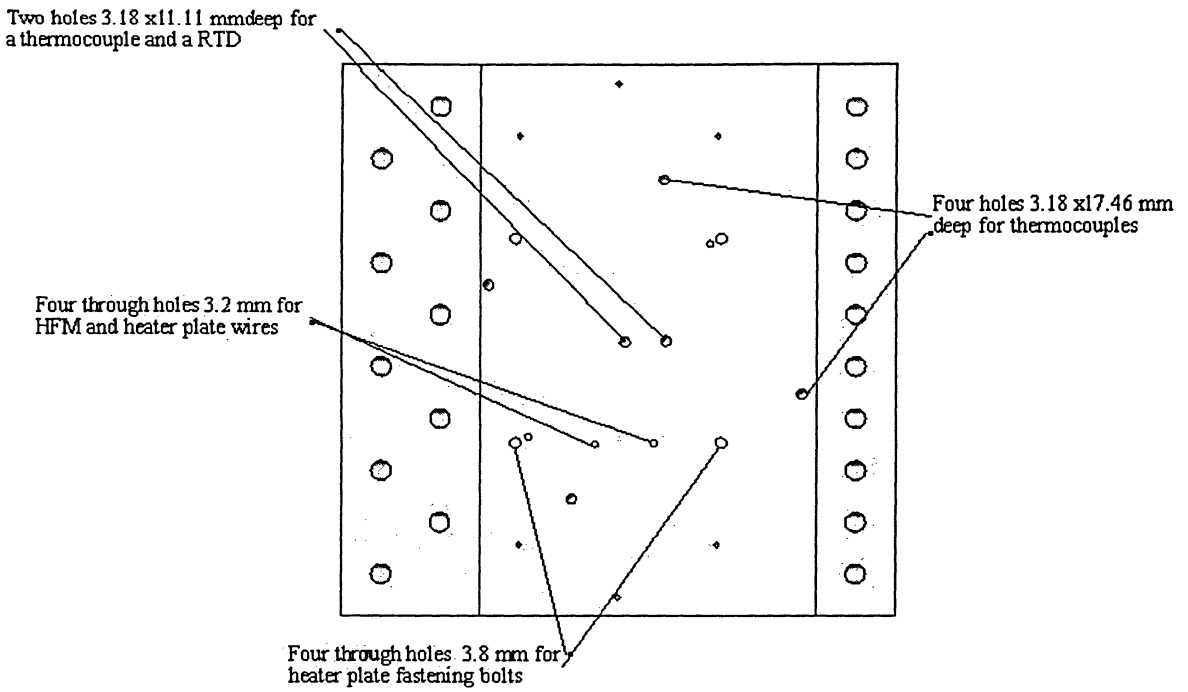

Figure 3-3 Back surface of hot plate with thermocouple, RTD and through holes.

3.2.1 Internal Flow Passages

As shown in Figure 3-2, ten through-passages with nominal diameter 6.35 mm (1/4 in.) and length 177.8 mm (7 in) are drilled across the width of each plate to form a bank of five laterals for a system of forward and return flow. A stream of heat transfer fluid entering the inlet header from the circulating bath will then flow into the five laterals, referred to as inlet laterals. The fluid from the inlet laterals then discharges into the crossover header. The heat transfer fluid in the crossover header then flows into the five other laterals, namely, the outlet laterals, which then enter the outlet header. This passage of the heat transfer fluid constitutes the flow through a single lateral of the flow system. For uniform temperature distribution throughout the plate, the inlet and outlet laterals are placed alternately across the length of the plate. The flow system allows the

circulating heat transfer fluid from a constant-temperature circulating bath to maintain uniform temperature of the plate.

The headers of the flow system are two copper bars which are drilled with through-holes, each with a nominal diameter of 18.26 mm (23/32 in.). One copper bar with dimensions 50.8 × 44.4 × 177.8 mm (2" × 1 3/4" × 7") is used to accommodate the inlet and outlet headers set up in a reverse flow arrangement. Another copper bar with dimensions 25.4 × 25.4 × 177.8 mm (1" × 1" × 7") is a cross connector for the laterals. The copper bars are soldered to the back surfaces of the plates, which were machined and pre-drilled with connecting holes to accommodate the copper bars. According to Bajura and Jones [16] and Datta and Majumdar [17], in general, a reverse flow arrangement has a better flow distribution than a parallel flow arrangement. Calculations showed (see Chapter 5) that the reverse flow manifold in Figure 3-2 has a fairly uniform flow among the tubes. Although the flow rate through the first tube was about 3.4% higher than the last one, the flow rate through the other laterals was less than ±2% of the average flow rate of the manifold. This gives a temperature difference of only 0.01 K between the first and last laterals in the plates, even if T_m is as high as 200°C, with an average heat flux across the plates of 1675 W/m^2.

3.3 The Heater Plate

The heater plate, having a nominal heat transfer measurement area of 76.2 × 76.2 mm or 0.00581 m^2 and overall thickness of 3.28 mm is made up of two copper plates. It is designed to maintain a high degree of temperature uniformity. A serpentine groove 3.18 mm wide by 1.59 mm deep, running up and down the plate with 18.4 mm spacing, as depicted in Figure 3-4, was machined into the thicker of the two plates, which is 2.13 mm thick. Sandwiched between the plates, but kept electrically

insulated from them, is a length of 26-gauge nichrome wire, 279 mm long and about 1.5 Ω in resistance. An air-drying ceramic paste, Omega Bond 600, which offers excellent electrical insulation and good thermal conductivity, surrounded the wire. The two plates were then soldered together, with the grooved surface on the inside, using a lead free solder with high liquidus temperature. Thus, the whole heater plate is essentially copper, helping to ensure a uniform temperature of the plate. The edge of the plate was chamfered to an angle of 45° so as to minimize heat transfer at the plate periphery. A two-dimensional numerical heat transfer analysis (see Chapter 4) showed that a temperature non-uniformity of less than 0.42% on the heater plate can be expected, even by a conservative estimate. The front side of the heater plate was machined flat to a tolerance of ±0.05 mm. Four through holes for 8-32 counter-sink bolts were machined into the grooved side of the heater plate through to the back surface. These 8-32 bolts, positioned at the corners, would then allow the heater plate to be drawn and bolted tightly against the heat flux meter on the hot plate.

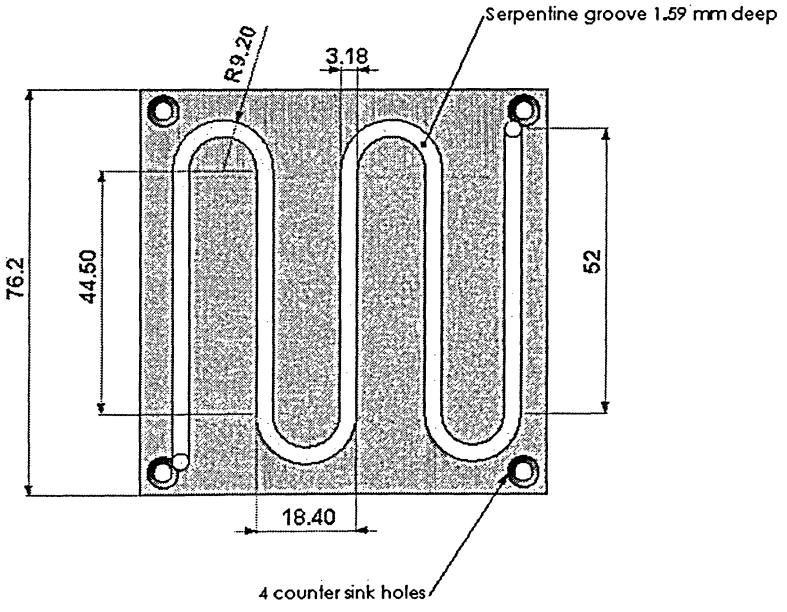

Figure 3-4 Heater plate serpentine groove and bolt holes.

3.3.1 The Heat Flux Meter

The heat flux meter (HFM) was manufactured by Technical Physiche Dienst T.N.O. of the Netherlands. It consisted of a silicone rubber disc 3.0 mm thick and 60.0 mm in diameter with approximately 800 thermocouples embedded in the center. One of the oldest techniques for the manufacture of the thermocouples is to wind constantan wire around a flexible plastic band (as Figure 3-5(a) illustrates) and plate one half of each winding with either pure copper or silver (Van der Graaf [18]). The junctions of the bare and the plated wires act as thermocouples and when connected in series, they form a thermopile, so as to measure the difference in temperature from one side of the disc to the other. The thermopile is woven into the centre of the disc, forming a sensitive zone of 50 mm in diameter, while the balance of the "non-sensitive" area of the disc, as illustrated in Figure 3-5(b) and (c), provides a guard for the thermopile to minimize measurement error. A heat flux across the sensor produced from a difference in temperature between the two sides of the disc induced a relatively large *emf* from the thermopile of approximately 1 mV per 4.78 W per m^2 of HFM area at 20°C. The thermal resistance of the HFM was approximately 4.25 K/W.

3.4 The Assembly of the Apparatus

The temperature difference between the hot and cold plates are obtained by five pairs of Type–T, Copper/Constantan (Cu/Cn), thermocouples which were embedded in the pre-drilled holes on each of the hot plate and the cold plate, attached together in series to form a thermopile. All thermocouples with the exception of the one used for the measurement of the heater-plate temperature were fabricated from 0.127-mm (36 gauge) Teflon insulated wires. Each thermocouple bead was first

electrically insulated with a thin coat of cured epoxy (Omegabond 200) and was then inserted to the bottom of the hole, which had been filled with epoxy. The temperatures of the hot and cold plate

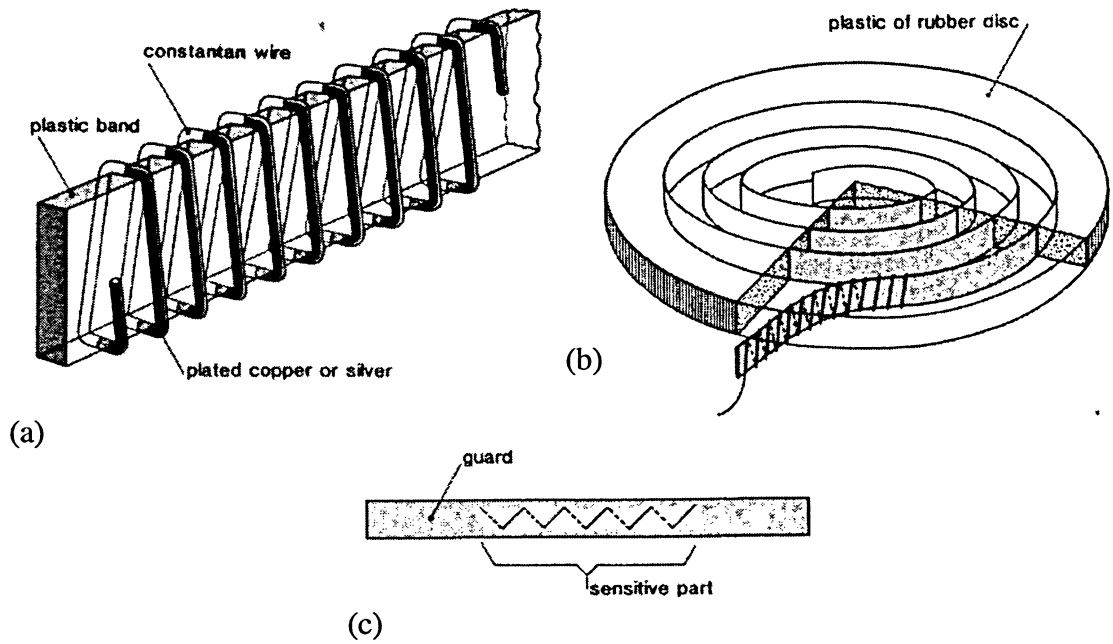

Figure 3-5 (a) Thermocouple wound on flexible band, (b) HFM with thermopile core and (c) Guarding of HFM (Van der Graaf [18]).

surfaces were measured by platinum resistance thermometers (RTD) with dimensions of $2.3 \times 2 \times 1$ mm (Omegafilm RTD, Series F) embedded in pre-drilled holes which had been filled with epoxy on the back surface of each plate. The wires of the RTDs and thermocouples were affixed to isotherms on the plate surfaces by epoxy for at least 80 mm in order to minimize the conduction error, as analyzed in Appendix B. The calibration and the measurement errors of the RTD's and thermocouples are presented in Appendix A and Chapter 6, respectively.

Before placing the heater plate and the HFM into the recess of the hot plate, a thermocouple, fabricated from 0.0762 mm (40-gauge) Teflon insulated Type-T copper/constantan (Cu/Cn) wires, was embedded in the back surface of the heater plate for measuring the surface temperature. The thermocouple wires were cemented on the back surface of the heater plate for about 80 mm to minimize conduction loss along the thermocouple wires (see Appendix B). The assembly of the heater plate and the HFM into the recess on the hot plate, as illustrated in Figure 3-6, required that the wires attached to the heater plate, the HFM and the thermocouple were first pulled through the holes to the back side of the hot plate. A thin film of thermal paste, Wakefield Engineering Inc. Thermal Compound, was applied to both sides of the HFM to ensure good thermal contact when sandwiched between the heater plate and the hot plate. The four bolts from the heater plate were then passed through to the back surface, where they were used to position the heater plate on the hot plate. To secure the heater plate and the HFM in place, nuts were screwed onto each of the heater plate's four bolts. Also, a 1 mm thick nylon spacer was inserted onto each bolt to thermally insulate the heater plate from the hot plate. Before tightening the nuts to draw the heater plate firmly against the HFM, so as to ensure good thermal contact, brass shims were used to assure equal spacing around the heater plate in the recess of the hot plate. The average spacing between the hot plate and the periphery of the heater plate was about 0.78 mm.

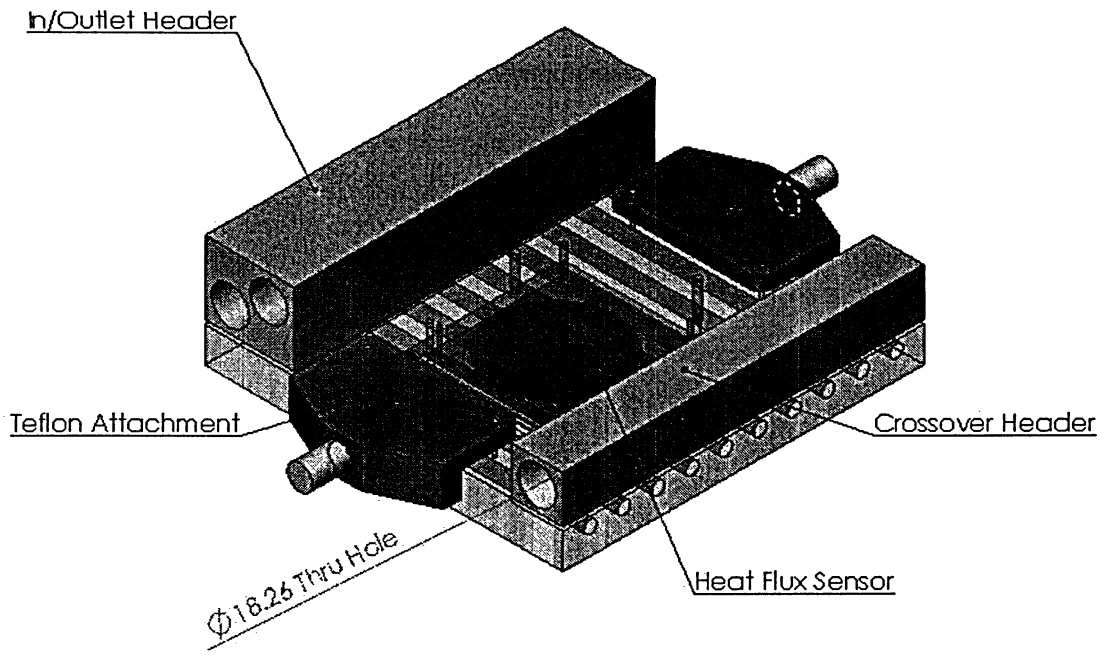

Figure 3-6 3-D sketch of the assembled Hot Plate

Finally, the assembled plates were mounted onto a frame with two self leveling supports made of Teflon plastic, which is capable of withstanding the high temperature expected of the apparatus. Because of the relatively low thermal conductivity of Teflon, the heat exchange between the assembly and the frame would be negligibly small. After the assembly was secured, hydraulic hoses were screwed into opposite ends of the inlet/outlet headers, with a coat of pipe dope applied to prevent circulating heat transfer fluid from leaking. The hoses were connected to the headers from the circulating baths through Parker's Quick-Connect couplings. When service is required, this type of coupling will allow easy detachment of the assembly from the circulating baths. After connecting all hydraulic lines the remaining openings on the headers and plates are plugged and checked for leaks. All wires for the sensors and the power supply were connected to terminal blocks on the frame, which were then connected to a data acquisition unit, power supply and computer.

A robust computer program – Hot Plate_Control – was written in Microsoft Visual Basic 6.0 (see Appendix C) to interact between the apparatus and the various supporting equipment. This program automates the experiment, monitoring critical parameters, as well as performing data acquisition and reduction when steady state is achieved.

CHAPTER 4

TEMPERATURE DISTRIBUTION ANALYSIS OF THE HEATED PLATES

4.1 Introduction

A finite element analysis (FEA) was done for the heated (hot, cold and heater) plates temperature distribution. A commercially available software, FEHT_Wiley – "Academic Version", was used for this analysis. The far-field effects of temperature nonuniformities were evaluated for various plate sizes and soil specimen thicknesses. The optimal size configuration (specimen thickness and diameter) was chosen from this evaluation to minimize the overall experimental error. For simplicity, the analysis was done with axisymmetric circular dimensions, even though the plates are square by design. The axisymmetric radii used were half the diagonal length of both the main plates and the heater plate, as illustrated in Figure 4-1, along with the diameter of the specimen container.

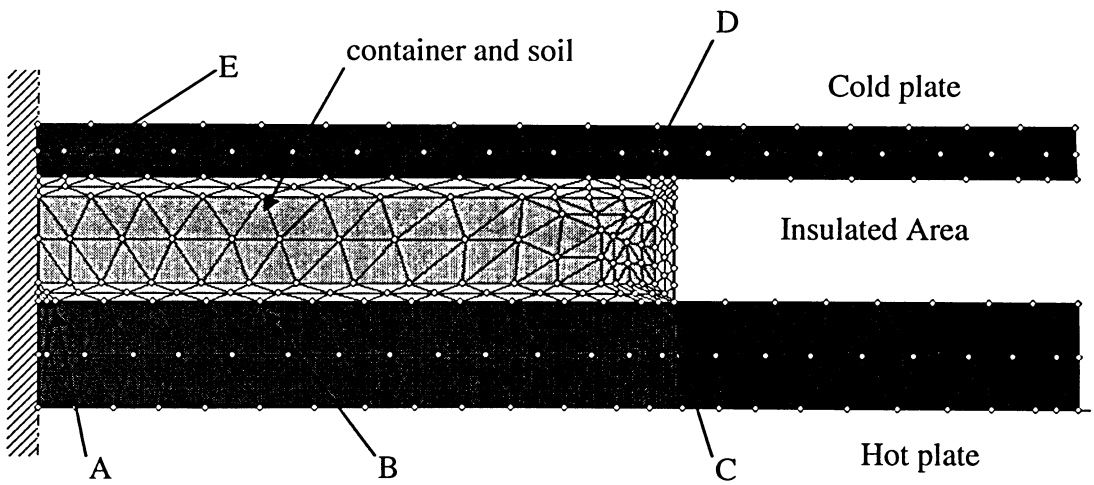

Figure 4-1 Triangular discretised grid of the plate assembly

The nodes identified in Figure 4-1 by letters A through to E, represents the temperature points used in the evaluation to follow. The area between nodes A and B represents the heater plate attached to the hot plate.

4.2 Method of Analysis

A two-dimensional analysis was done on a triangular discretised finite element grid over the plate's geometrical domain. The steady-state heat-conduction equation, Eq. (4.1), is then solved numerically over this domain.

$$\nabla^2 T = 0 \qquad \textbf{(4.1)}$$

The evaluation was done at a high temperature (200°C) since the largest temperature nonuniformities occur at high surface temperatures as well as for a high temperature difference. The equation was solved for high plate surface temperature, with the temperature difference between hot and cold plates of 10 K, which is the worst-case scenario for the experiment. The specimen under investigation for this analysis is soil, which represents the primary application of the apparatus. Also, with the axisymmetric radii being the longest dimension, the results produced are considered conservative.

The analysis was set up such that the symmetric boundaries were considered adiabatic; surfaces of the plates not in contact with the specimen container were also considered adiabatic (insulated area of Figure 4-1). A uniform heat flux of 1675 W/m^2, derived from the average heat transfer coefficient deduced in Chapter 5, was assumed for the flow system in the plates. The locations for the heat flux from the flow system were placed on the back surface of the main plates according to the locations of the internal flow passages and areas between these locations were assumed adiabatic. A high thermal conductivity of 2.52 W/mK was chosen for the soil for more conservative results as well values of

56.7 W/mK and 393 W/mK were used for the electro-plated steel container and the main plates, respectively.

4.3 Analysis Results

A grid refinement study was also done for the discretised domain, using a "Fully Licensed Version" of the FEHT_Wiley software. The number of nodes was increased by as much as three times over the number used in the initial evaluation. The temperature variations (derived when the number of nodes was increased for the grid refinement study) were shown to be independent of the number of nodes. Therefore, the "Academic Version" of the software had sufficient nodes for this analysis.

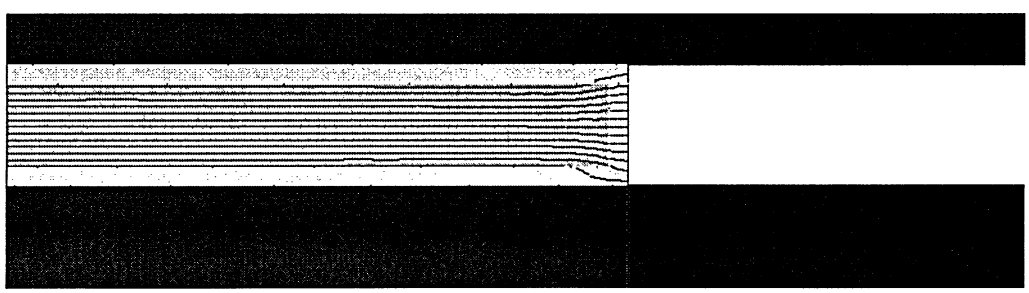

Figure 4-2 Isothermal lines of the numerical evaluation for ΔT of 10 K

The numerical results show that the temperature distributions in the plates (Figure 4-2) remain practically uniform and one dimensional, even for the worst-case situation. The isotherms, for maximum and minimum temperatures of 462.8 and 472.1K, as shown in Figure 4-2, are uniform in the region of the metering area (between nodes A and B), thus ensuring uniform one-dimensional heat flow through the soil sample, for the conditions assumed. The disturbance to the heat flow in the region between nodes B and C, caused by the soil sample container (described in Chapter 7), will not

adversely affect the thermal conductivity measurement. It is this disturbance that causes a higher nonuniformity in the hot and cold plate temperatures than in the heater plate temperature.

The temperature nonuniformities for the plates were evaluated by

$$\frac{\delta T}{\Delta T} = \frac{T_0 - T_1}{2\Delta T} \tag{4.2}$$

where T_0 and T_1 are high and low temperatures, respectively on the surface of a plate, and $(T_0 - T_1)$ is given by $(T_A - T_B)$, $(T_A - T_C)$ and $(T_E - T_D)$ for the heater, hot and cold plates respectively. The temperature nonuniformities for a mean temperature of 473 K and ΔT of 10 K were found to be 0.88%, 1.87% and 0.42% for the hot, cold and heater plates respectively, i.e., for $(T_0 - T_1)$ of 0.176, 0.373 and 0.084K for the hot, cold and heater plates respectively. This temperature nonuniformity corresponds to a flow rate of 10.863 L/min of heat transfer fluid through the flow system, container thermal conductivity of 56.7 W/mK and soil thermal conductivity of 2.52 W/mK.

CHAPTER 5

FLOW DISTRIBUTION MANIFOLD ANALYSIS

5.1 Introduction

An analytical description of the internal flow passages of the main (hot and cold) plates is given in this section. The plates are maintained at constant temperatures by the passing of a stream of heat transfer fluid through the flow system machined in the plates. A reverse flow arrangement was designed on the basis of achieving maximum fluid flow while minimizing the pressure drop in the system, for a better temperature distribution through these plates. A reverse flow system, as shown in Figure 5-1, is a combination of two simple manifolds, namely, dividing and combining flow manifolds interconnected by lateral branches.

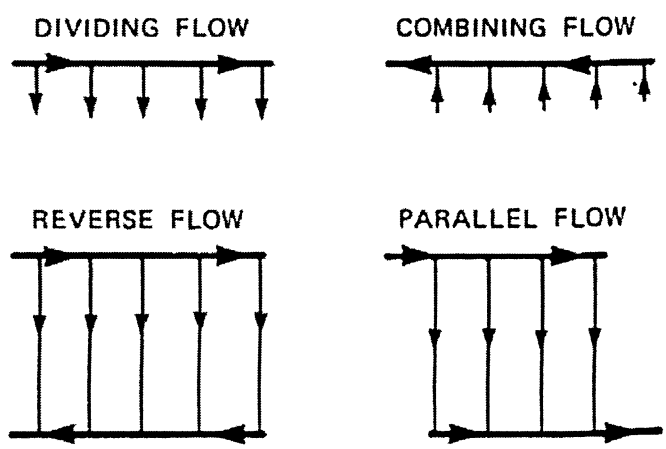

Figure 5-1 Four basic types of flow manifolds (Bajura and Jones [16])

5.2 Manifold Analysis

A manifold is a flow passage with porous sidewalls (laterals) through which fluid enters or leaves as a result of a differential pressure. In a dividing flow header, there is a decrease in the flow of the main fluid stream due to the loss of fluid through the laterals. Therefore, there will be an increase of pressure in the direction of flow if the effects of friction are small, which can be demonstrated by applying a frictionless Bernoulli equation to the header flow stream. However, in a combining flow header, pressure decreases in the direction of the main fluid steam. This drop in pressure occurs as a result of the additive effects of both the frictional pressure losses and the favorable pressure gradient required for acceleration of the main stream, due to inflow at the branch points. Assuming a one-dimensional flow field, the governing equations for the flow system are the continuity and momentum equations for each header and the discharge equation for the lateral flows. The work-energy equation can also be applied to the header flow stream, after applying the appropriate assumption.

A continuous flow model can analyze the lateral flows for a manifold with many branch points. However, for this model, the discrete branch points are first defined then applied to a reverse flow system. Figure 5-2 is an illustration of a control volume for a flow stream near a dividing flow branch point. The stream of fluid at surface A_{31} has velocity components V_x and V_y, since it is assumed that the discharge has not turned completely 90 degrees when crossing the boundary of the control volume. The length of the control volume Δx_1, in the direction of the fluid stream is derived by dividing the axial length, L_1, by the total number of branch points, N_1. The following assumptions are applied through the analysis:

1. The lateral area at the branch point, A_{31}, is constant along the header.
2. The branch points are uniformly distributed along the header.
3. The fluid is incompressible.

4. The header area, A_1, is constant.

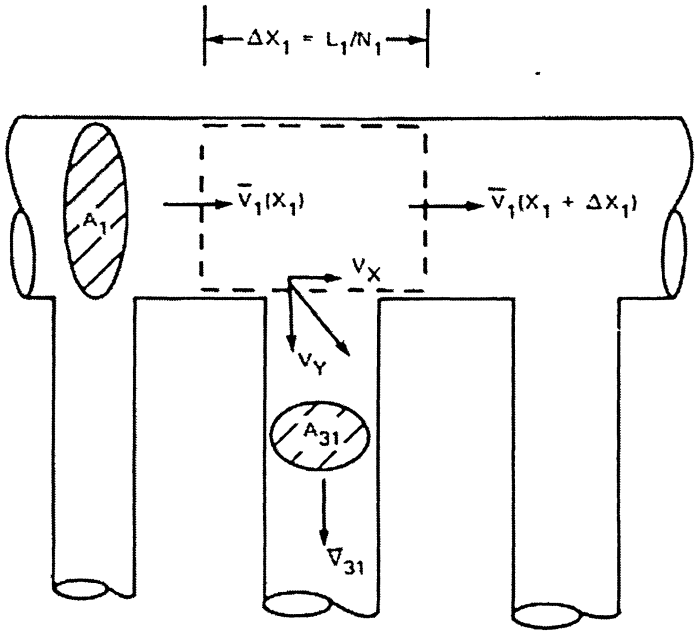

Figure 5-2 Dividing flow branch point control volume (Bajura and Jones [16]).

The flow condition at $(x_1 + \Delta x_1)$ according to Bajura and Jones [16] is related to the flow condition by x_1 at a first order Taylor series expansion. The continuity equation for the control volume is

$$V_{31}A_{31} = -A_1 \frac{dV_1}{dx_1} \frac{L_1}{N_1} \tag{5.1}$$

where V_{31} and V_1 are average velocities in the lateral and header, respectively. The momentum equation for the control volume is given by

$$\frac{1}{\rho}\frac{dP_1}{dx_1} + \left(\frac{f_1\pi_1}{8A_1} + \frac{d\beta_1}{dx_1}\right)V_1^2 + \theta_1 V_1 \frac{dV_1}{dx_1} = 0 \tag{5.2}$$

where β_1 is an axial flow momentum correction factor, θ_1 is an overall momentum correction factor, f_1 is the Moody friction factor and P_1 is the pressure. These parameters are formally defined by

Bajura and Jones [16], as well as the complete manifold analysis, which is summarized in this section for a reverse flow system.

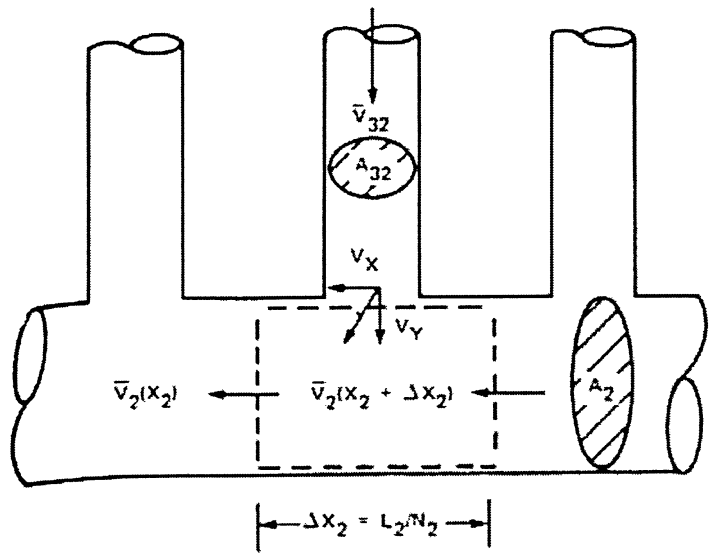

Figure 5-3 Combining flow branch point control volume - pertinent to a reverse flow system (Bajura and Jones [16]).

The control volume illustrated in Figure 5-3 is for the analysis of a combining flow manifold, for a reverse flow system. Using an analysis similar to the dividing flow header above, the momentum equation is given by

$$\frac{1}{\rho}\frac{dP_2}{dx_2} + \left(-\frac{f_2\pi_2}{8A_2} + \frac{d\beta_2}{dx_2}\right)V_2^2 + \theta_2 V_2 \frac{dV_2}{dx_2} = 0 \qquad \textbf{(5.3)}$$

The friction term is negative in Eq. (5.3), since the flow direction is defined as being positive in the negative x_2 direction. The equations above now have four unknowns, namely, the pressures P_1 and P_2 and the velocities V_1 and V_2. To ensure the flow from one header enters the other, the velocities are related by an inter-manifold continuity equation, which is given by

$$V_2 = V_1(A_1/A_2) \qquad \textbf{(5.4)}$$

A discharge equation pertaining to the control volume illustrated in Figure 5-4 is developed for the relationship between the pressure differential between manifolds and the lateral flow rate as follows:

$$\frac{P_1}{\rho} = \frac{P_2}{\rho} + H\frac{V_{31}^2}{2} \tag{5.5}$$

where the lateral flow resistance, H is given by

$$H = C_{TD} + K_{eq} + (fl/d)_{eq} + (1 + C_{TC})\left(\frac{A_{31}}{A_{32}}\right)^2 \tag{5.6}$$

The terms C_{TD} and C_{TC} are turning loss coefficients for dividing and combining flows, respectively as evaluated in Table 5-1. the terms K_{eq} and $(fl/d)_{eq}$ represent the equivalent loss coefficient (based on velocity V_{31}) for local upset flow and frictional losses. These loss coefficients were evaluated for turbulent flow in smooth pipe and the Colbeck-White correlation was used for the frictional loss coefficient. When the overall flow resistance becomes large, the turning loss terms assume minor significance in the discharge equation.

Table 5-1 Evaluation of loss coefficients for the flow system (Potter *et al.* [19] and Graebel [20]).

Terms	Descriptions	Evaluations
C_{TC}	Combing Loss	$(1- A_2/A_1)^2$
C_C	Vena Contracta	$0.62 + 0.38(A_2/A_1)^3$
C_{TD}	Dividing Loss	$((1 - C_C)/C_C)^2$
f	Frictional Loss	$1/(1.82\times\log_{10}(Re)) - 1.64)^2$

where Re is the Reynolds Number for the fluid flow.

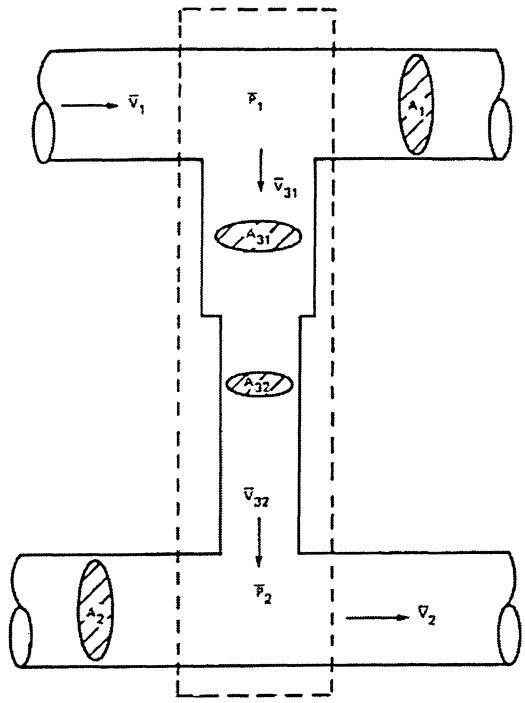

Figure 5-4 Lateral flow control volume (Bajura and Jones [16])

Eqs. (5.1) and (5.5) may be manipulated for a relationship between the differential pressure and flow rate in the dividing flow header and solved for the velocity gradient as follows:

$$\frac{dV_1}{dx_1} = -\frac{N_1 A_{31}}{A_1 L_1}\left(\frac{2}{\rho H}\right)^{1/2} (\Delta P_{12})^{1/2} \tag{5.7}$$

where $\Delta P_{12} = (P_1 - P_2)$, is the differential pressure between headers. The minus sign is used since the velocity V_1 must decrease with distance x_1. This condition requires that the pressure differential always be positive, or a reversal of flow will occur.

A careful manipulation of Eqs. (5.2), (5.3), (5.4) and (5.7) yields a set of first order equations called the Pressure-Flow Equations. First Eq. (5.3) is subtracted from Eq. (5.2) to obtain an equation in terms of the differential pressure, ΔP_{12}, between headers. The resulting equation is then solved with Eq. (5.4) to eliminate the velocity V_2 term. Finally the remaining equations are nondimensionalized,

according to Bajura and Jones [16], by the following reference quantities: the entrance velocity to the dividing flow, V_{10}; the length of each header, L_1 and L_2; and the entering flow rate Q_0, producing the dimensionless Pressure-Flow Equations:

$$\frac{dV}{dx} = -\frac{N_1 A_{31}}{A_1}\left(\frac{2}{H}\right)^{1/2} (\Delta P)^{1/2} \tag{5.8}$$

$$\frac{d(\Delta P)}{dx} = -\left[\frac{f_1 L_1 \pi_1}{8A_1} + \frac{f_2 L_2 \pi_2}{8A_2}\left(\frac{A_1}{A_2}\right)^2 + \frac{d\beta_1}{dx} - \frac{d\beta_2}{dx}\right] V^2 - \left[\theta_1 - \theta_2\left(\frac{A_1}{A_2}\right)^2\right] V \frac{dV}{dx} \tag{5.9}$$

which must satisfy the following boundary conditions: at the inlet, the dimensionless velocity V must equal 1; and at the dead end of the manifold, a physical condition imposed by the manifold wall, the velocity V is zero.

If the differential pressure is eliminated from Eqs. (5.8) and (5.9), a second order equation in the dimensionless flow rate Q can be obtained as:

$$\frac{H}{A_R^2} Q'Q'' + \left[\frac{d\beta_1}{dx} - \frac{d\beta_2}{dx}\right] Q^2 + \left[\frac{f_1 L_1 \pi_1}{8A_1} + \frac{f_2 L_2 \pi_2}{8A_2}\left(\frac{A_1}{A_2}\right)^2\right] Q^2 + \left[\theta_1 - \theta_2\left(\frac{A_1}{A_2}\right)^2\right] QQ' = 0 \tag{5.10}$$

where $A_R = N_1 A_{31}/A_1$ is the area ratio of the manifolds, which is the total lateral cross-sectional area to the cross-sectional area of the header. Eq. (5.10) is a flow distribution equation and is subject to the following boundary conditions: $Q(0) = 1$ and $Q(1) = 0$.

5.3 Calculations and Results

The flow distribution equation was used to analyze the header to lateral combination for the plates' flow system. The header to lateral combination was chosen to give maximum flow, thus minimizing the temperature difference, in effect minimizing the error in the apparatus. The analysis was done for a flow system with header and lateral diameters of 18.26 mm and 6.35 mm, respectively, with five (5) equally spaced laterals each of length 356.82 mm, as shown in Figure 5-5 and evaluated in Table 5-2. The pipe turning loss coefficient was evaluated according to a correlation derived in several Fluid Mechanics texts (such as Wang [21], Potter *et al* [19] and Saleh [22], while turbulent correlations taken from Graebel [20]), were employed for the frictional losses used throughout the analysis. All calculations were done with Waterloo_Maple 7.

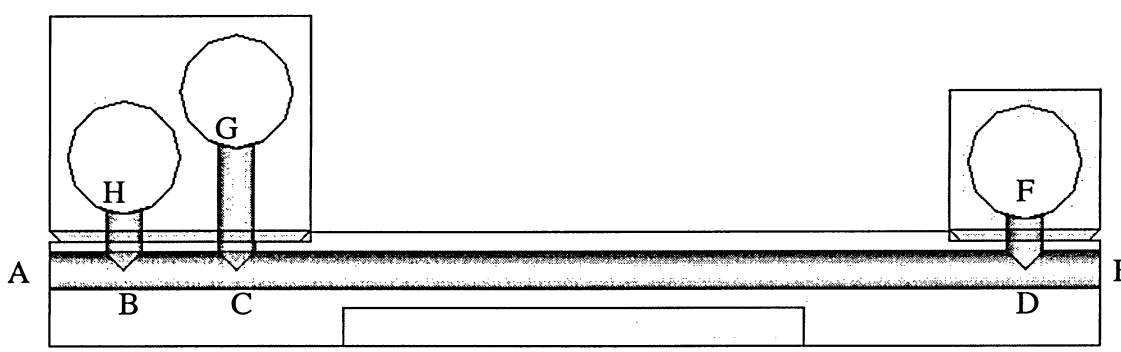

Figure 5-5 Lateral length evaluation points.

The evaluation of the manifold system was done with an inlet flow rate of 10.863 L/min from the circulating bath filled with Calflo LT at 200°C. The manifold was shown to have an average flow rate of 2.173 L/min with a maximum of 3.5 percent difference in the flow between the first and last laterals. This flow condition will produce a maximum of 1.87 percent difference in the plate

temperature (cold plate), as derived from the heat transfer coefficient of the circulating fluid in the first and last laterals and the numerical analysis of Chapter 4.

Table 5-2 Lateral length evaluation as shown in Figure 5-5, all dimensions are given in millimeters.

Location	Description	Distance	Total
A – E	Through holes across the plate width	2×177.8	
B – H	Inlet header connector	20.65	
C – G	Outlet header connector	31.75	
D – F	Crossover header connectors	2×17.61	443.22
F – F	Distance between inlet and outlet lateral	-16.6	
A – B	Plate edge to inlet header	-12.7	
A – C	Plate edge to outlet header	-31.7	
D – E	Plate edge to crossover header	-2×12.7	-86.4
Total length of lateral			356.82

CHAPTER 6

MEASUREMENT ERROR ANALYSIS

6.1 Introduction

The overall uncertainty in measurements or derived quantities is a combination of errors from various sources. Calibration, signal conditioning, data acquisition, and data reduction are a few of the sources considered in this analysis. The methodology as outlined by Leong [13] for deriving the overall uncertainty in a measurement or in a derived quantity is reviewed in this section.

6.1.1 Uncertainty in Measurements

For each measurement, i, the total error, δ_i, is considered to be comprised of two components: a bias error (β) and a precision error (ε_i), such that:

$$\delta_i = \beta + \varepsilon_i \qquad (6.1)$$

The bias error, which is not based on a statistical estimate, is assumed to be constant for repeated measurements of a given variable. Therefore, it represents a fixed deviation from the true value estimated using a degree of judgment with the assistance of calibrations and/or independent measurements. However, the precision error is based on statistical considerations and is given by the standard deviation (σ) of a parameter population. The precision index of a measurement (S_x) for N

repeated measurements of a parameter x, which is the best estimate of σ, is also known as the standard error and is given by

$$S_x = \left(\frac{\sum_{i=1}^{N} (x_i - \bar{x})^2}{N-1} \right)^{1/2} \qquad \textbf{(6.2)}$$

where $\bar{x}$ is the mean of the x_i measurements.

Since the overall uncertainty in measurement will be associated with the mean value, the precision index of the mean is needed in the analysis of uncertainties.

$$S_{\bar{x}} = \frac{S_x}{\sqrt{N}} \qquad \textbf{(6.3)}$$

The number of degrees of freedom, υ, given by N-1, for the precision index of a measurement also applies to the precision index of the mean.

The errors from 'j' categories for the measurement of an individual parameter are combined using the root-sum-square (RSS) method. Thus, the total bias error of the parameter x is given by

$$\mathbf{B_x} = \left[B_1^{\,2} + B_2^{\,2} + \ldots + B_j^{\,2} \right]^{1/2} \qquad \textbf{(6.4)}$$

and the precision index of the parameter is given by

$$S_x = \left[(S_x)_1^2 + (S_x)_2^2 + \ldots + (S_x)_j^2\right]^{1/2} \quad (6.5)$$

Combining the bias and precision errors gives the range within which the true value of the parameter should lie. This range is representative of the overall uncertainty (U) in the parameter. The RSS uncertainty method, which is associated with the 95% confidence level, used for combining these errors is given by:

$$U_{0.95} = \left[(B_x)^2 + (t'S_{\bar{x}})^2\right]^{1/2} \quad (6.6)$$

Here t' is the Student's t multiplier for 95% confidence and υ degrees of freedom.

6.1.2 Uncertainty in Derived Quantities

The determination of the uncertainty in a derived result must include the relationship between the result and the independent parameters. This functional dependence is indicated by sensitivity coefficients, θ. For a relationship

$$Y = f(X_1, X_2, \ldots, X_K) \quad (6.7)$$

the sensitivity coefficient is given by

$$\theta_i = \frac{\partial Y}{\partial X_i} \quad (6.8)$$

The bias error of the derived result is then given by

$$B_Y = \left[\sum_{i=1}^{K} (\theta_i B_i)^2\right]^{1/2} \tag{6.9}$$

and the precision index of the derived result is given by

$$S_Y = \left[\sum_{i=1}^{K} (\theta_i S_i)^2\right]^{1/2} \tag{6.10}$$

The number of degrees of freedom υ_Y is N-1, where N is the number of measurements in the data set, assuming each parameter was measured the same number of times.

The Student's *t* multiplier (based on the two-tailed distribution) is next found at the 95% confidence level, and the uncertainty in the result is then determined by

$$(U_Y)_{0.95} = \left[(B_Y)^2 + (t' S_Y)^2\right]^{1/2} \tag{6.11}$$

This is the interval around the derived result Y within which the true value is believed to lie.

6.2 Instrumentation Specifications

The specifications for the instrumentation associated with the calibration of the apparatus and with the experiment are summarized in Table 6.1.

Table 6.1 Instrumentation specifications

a) Voltage Conditioner Card:

i) Daytronic Model 10A65-8, 8-Channel Low-level Analog Card

Range	Resolution	Error (1 year specifications)	
		Bias (%)	Precision (%)
±50 mV	24 μV	0.02% of reading	100 μV
±100 mV	49 μV	0.02% of reading	100 μV
±200 mV	98 μV	0.02% of reading	100 μV

ii) Daytronic Model 10A9-8C, 8-Channel Thermocouple Card

Range	Resolution	Error (1 year specifications)	
		Bias (%)	Precision (%)
±80 mV	44 μV	0.05% of reading	100 μV

b) Temperature

i) Platinum Resistance Thermometer (PRT)
Model: Azonix Corporation Model 12001A-1262A, Laboratory grade
Repeatability plus Accuracy: 0.006°C

ii) Platinum Resistance Temperature Detector (RTD)
Model: OMEGAFILM RTD Element Series F, Catalog No. F3105
Nominal Resistance: 100 Ω at 0°C
Repeatability: < 0.01°C

iii) Standard 1-mA Current Source
Stability: ± 0.0015 mA ($T_{ambient}$ = 25°C ± 5°C)

c) NEMIC-LAMBDA Programmable Power Supply
Model: ZUP 10-20

i) Constant Voltage
Range: 0 to 10 V with 2.8 mV resolution
Stability: ± 0.01% + 2 mV ($T_{ambient}$ = 25°C ± 5°C)

ii) Constant Current
Range: 0 to 20 A with 6 mA resolution
Stability: ± 0.02% + 5 mA ($T_{ambient}$ = 25°C ± 5°C)

d) Starrett Micrometers
Range: 0 to 25.4 mm and 0 to 200 mm
Precision error (s): 0.0254 mm

6.3 Measurement of Plate Temperatures

Two Omegafilm Series F platinum resistance temperature detectors (RTDs) were used to measure the surface temperatures of the main plates. Each RTD has a nominal resistance of 100 ohms at 0°C and dimensions of 2.3 × 2 × 1 mm. These RTDs were connected in series to a 1-mA standard current source. A platinum resistance thermometer, PRT (Azonix Corporation Model 12001A-1262A), designed for high accuracy laboratory measurements was used for the calibration of the RTDs. The accuracy of the PRT is stated to be ±0.006°C. The temperature of the hot plate (or the cold plate) used in the data analysis was that of the RTD on each of the plates. The RTDs were inserted to within 1.59 mm of the front plate surface in 3.18 mm diameter holes, which had previously been filled with epoxy. The four lead wires (36-gauge Teflon insulated copper wire) of each RTD were bonded with epoxy to the plate for a minimum 80 mm distance from the hole.

During the calibration procedure, the temperature of the heater plate was measured using an Omega 40-gauge Copper/Constantan (type-T) thermocouple. The Daytronic System 10 unit has a card for directly converting thermocouple output to temperature. The thermocouple was also calibrated against the PRT in the same way as for the RTDs. Using least squares analysis, a sixth order polynomial fit was obtained between the PRT's temperature and the thermocouple's temperature. The maximum fit error was 0.02 K. From an error analysis, it was concluded that the error in temperature caused by the use of the Daytronic System 10 unit and the fitted equation for the thermocouple was ±0.034 K. The thermocouple was inserted into a 1.59 mm diameter by 2.6 mm deep hole, which had been previously filled with epoxy, located 25 mm from one corner of the back surface of the heater plate and 4 mm away from the edge. The thermocouple wires were affixed by epoxy to the plate for a 80 mm distance from the hole.

Measurement of a characteristic temperature must include an estimate of the temperature nonuniformity of the body being measured, as well as the conduction error associated with the wire. Thus, from Chapters 4 and 5 and Appendix B, the overall bias errors for measuring the temperature of the hot plate, the cold plate, and the heater plate were given, respectively, by the following:

i) For the hot plate as measured by a RTD with four lead wires (36 gauge), the bias error is evaluated from (a) the fluid temperature change, (b) the conduction error due to lead wires, and (c) the calibration of the RTD, and is given by:

$$B(T_h) = \left[(0.0017\Delta T)^2 + (4\times 0.0016)^2 + (0.0283)^2\right]^{1/2} \qquad \textbf{(6.12)}$$

ii) For the cold plate as measured by the RTD with four lead wires (36 gauge), the items are similar to the $B(T_h)$, and the bias error is given by:

$$B(T_c) = \left[(0.0033\Delta T)^2 + (4\times 0.018)^2 + (0.0283)^2\right]^{1/2} \qquad \textbf{(6.13)}$$

iii) For the heater plate as measured by a thermocouple (40-gauge), the bias error is due to (a) heater plate temperature nonuniformity due to the HFM, (b) the conduction error due to the thermocouple lead wire, and (c) the calibration of the thermocouple, and is given by:

$$B(T_{htr}) = \left[(0.0011\Delta T)^2 + (0.0011)^2 + (0.034)^2\right]^{1/2} \qquad \textbf{(6.14)}$$

For the maximum ΔT of 10 K used in the experiments, the maximum overall bias limits for measuring temperatures of the hot plate, the cold plate, and the heater plate were obtained to be ±0.0336 K, ±0.0841 K, and ±0.0358 K, respectively.

Using the RRS method, the bias error of the mean temperature T_m between the hot plate and the cold plate was obtained as

$$\frac{B(T_m)}{T_m} = \left[\left(\frac{0.00586}{T_m}\right)^2 + 2.89\times10^{-6}\left(\frac{\Delta T}{T_m}\right)^2\right]^{1/2} \qquad \textbf{(6.15)}$$

Since the mean temperature was in the order of 473 K, the overall bias error in the mean temperature was negligibly small over the experimental range of ΔT and T_m.

6.4 Measurement of Temperature Differences

The temperature difference between the hot and cold plates was measured using Cu/Cn thermopile. The thermopile contained five (5) thermocouple pairs, which, for a nominal Cu/Cn sensitivity of 40 μV/K each, permitted measurement of temperature difference with a resolution of ±0.012 K (Burns [23]). Each thermocouple was fabricated in-house from 36-gauge Cu and Cn wires by tightly twisting the ends and coating the Cu/Cn junction with a thin layer of Envirobrite solder. A thin coat of epoxy, which was allowed to cure, electrically insulated the thermocouple beads. One end of each thermopile was inserted to within 1.59 mm of the front surfaces of both the hot and cold plates in a 3.18 mm hole. The thermocouple wires were bonded with epoxy to the plates for a distance of at least 80 mm distance from the hole.

The thermopile voltage was converted to a temperature by the following steps (Leong [13]):

1) A reference voltage in μV for the reference temperature, T_{ref}, at the hot side of the thermopile was calculated for a 0°C base using the following relationship for 0°C $\leq T_{ref} \leq$200°C to ±0.01 μV (Burns [23]):

$$V_{ref} = 38.7481T_{ref} + 3.3292\times10^{-2}\,T_{ref}^{2} + 2.0618\times10^{-4}\,T_{ref}^{3} - 2.1882\times10^{-6}\,T_{ref}^{4} + 1.0997\times10^{-8}$$

$$T_{ref}^{5} - 3.0816\times10^{-11}\,T_{ref}^{6} + 4.5479\times10^{-14}\,T_{ref}^{7} - 2.7513\times10^{-17}\,T_{ref}^{8} \qquad \textbf{(6.16)}$$

2) The measured voltage, V, from the thermopile was divided by the number of thermocouple pairs, N = 5, and converted to μV:

$$V_{m} = \left(\frac{V}{N}\right)\times10^{6} \qquad \textbf{(6.17)}$$

3) An equivalent Cu/Cn voltage for a reference temperature of 0°C was calculated as the sum of V_{m} and V_{ref}:

$$V_{eq} = V_{m} + V_{ref} \qquad \textbf{(6.18)}$$

4) The equivalent voltage V_{eq} in μV was converted to a temperature, T, using the following relationship for 0°C $\leq$ T$\leq$ 200°C to ±0.001°C:

$$T = 0.025928V_{eq} - 7.60296\times10^{-7}\,V_{eq}^{2} + 4.63779\times10^{-11}\,V_{eq}^{3} - 2.165392\times10^{-15}\,V_{eq}^{4}$$

$$+ 6.04814\times10^{-20}\,V_{eq}^{5} - 7.29342\times10^{-25}\,V_{eq}^{6} \qquad \textbf{(6.19)}$$

5) Finally the temperature difference measured by the thermopile is given by

$$\Delta T = T - T_{ref} \qquad \textbf{(6.20)}$$

The largest uncertainty in the measurement of the temperature difference using the thermopile was the uncertainty of the reference temperature. Therefore, the bias limit for measuring the temperature

difference between the hot and cold plates using the thermopile was the RSS of $B(T_{ref})$ (i.e., either $B(T_h)$ or $B(T_c)$), the conduction error, and the conversion errors in Steps 1 and 4 above:

$$\frac{B(\Delta T)}{\Delta T} = \left[\left(\frac{0.0621}{\Delta T}\right)^2 + 2.89\times10^{-6}\right]^{1/2} \qquad \textbf{(6.21)}$$

The bias error of the ΔT at 10 K between the hot and cold plates, using the thermopile and the hot plate temperature as the reference was 0.644%.

6.5 Measurement of Electrical Power

The power to the heater plate was supplied by a NEMIC-LAMBDA Power Supply (Model ZUP 10-20). This unit has a programmable constant-voltage operation with resolution better than 3 mV. A piece of constantan wire with resistance (R_{sh}) of 0.1785 Ω ±0.022% was connected in series across the heater plate to form a shunt resistance. The current to the heater plate was determined from the shunt resistance. The voltage drops across the heater plate, V, and the shunt resistance, V_{sh}, were measured by the Daytronic System10 unit. Then, the electrical power supplied to the heater plate was determined by:

$$(VI) = V\left(\frac{V_{sh}}{R_{sh}}\right) \qquad \textbf{(6.22)}$$

Using the RSS method the bias error for measuring electrical power to the heater plate was determined by:

$$\frac{B(VI)}{VI} = \left[\left(\frac{B(V)}{V} \right)^2 + \left(\frac{B(V_{sh})}{V_{sh}} \right)^2 + \left(\frac{B(R_{sh})}{R_{sh}} \right)^2 \right]^{1/2} \qquad \textbf{(6.23)}$$

where $\frac{B(V)}{V} = \frac{B(V_{sh})}{V_{sh}} = \pm 0.02\%$ and $\frac{B(R_{sh})}{R_{sh}} = \pm 0.022\%$. The bias error of the electrical power to the heater plate is calculated to be ±0.036%.

6.6 Measurement of Other Dimensions

Measurements of other dimensions were required. These included the effective surface area of the heater plate A_{hp}, the distance between the hot plate and the cold plate *L*, the diameter *D*, and the height *H* of the specimen container. A Starrett Micrometer with a precision error of ±0.0254 mm was used for measurement of dimensions less than 25.4 mm and another for dimensions up to 200 mm. The micrometers were checked in the Mechanical and Industrial Engineering Department Machine Shop against standard length pieces and standard thickness blocks to confirm their precision errors. The steel straight edges used to determine plate flatness were checked against a standard granite plate. A light source held behind the straight edges did not reveal any deviations between the two surfaces. Each dimension was the average of ten measurements at different locations.

Effective Heater Plate Area

The effective heater plate area is defined as the area of a plate having sides equal to the heater plate side dimensions plus one-half the nominal 0.80 mm width of the gap between the plate and the hot

plate, and the uncertainty in this area was taken as one-half of the gap area. Therefore, the effective heater plate area was calculated to be

$A_{hp} = 5.929\times 10^{-3}\ m^2 \pm 1.232 \times 10^{-4}\ m^2$ (or ±2.08 % uncertainty).

Total Specimen Thickness

The linear distance between the hot and cold plates was taken as the sum of the filled thickness of soil layer in the specimen container, the thickness of the container base wall and lid, and the thickness of the thermal paste on both outer surfaces of the container. The total specimen thickness was calculated to be L = 21.58 mm ± 0.0254 mm (or ±0.118% uncertainty).

Effective Specimen Thickness

The effective specimen thickness is the filled thickness of soil layer in the specimen container, i.e., H = 20.83 mm ± 0.1059 mm (or ±0.508% uncertainty).

Other Dimensions

The other dimensions required in the analysis are:

Diameter of specimen container, D = 149.42 mm ± 0.0924 mm (or ± 0.062% uncertainty)

Thickness of specimen container base and cover, d = 0.23 mm ± 0.025 mm

Plate Flatness

Plate flatness was measured using steel straight edges and a precision feeler gauge set. The average deviation in the plate flatness was determined to be in the order of ±0.05 mm over the plate's surface. This deviation was measured by checking the thickness of the gaps between straight edges and the plates using a precision feeler gauge set.

6.7 Measurement of Heat Flux

The heat transfer from the heater plate to the cold plate is given by

$$q = q_e - q_b \tag{6.24}$$

where q_e is the power to the heater plate given by *VI*, and q_b is the back heat transfer through the HFM, given by αe.

Hence, the heat flux through the specimen is determined by:

$$q'' = \frac{q}{A_{hp}} = \frac{VI - \alpha e}{A_{hp}} \tag{6.25}$$

where A_{hp} is the effective heater plate area. However, the emf of HFM is practically equal to zero for achieving isothermal condition between the heater and hot plates; hence, the heat flux is essentially equal to:

$$q'' = \frac{VI}{A_{hp}}$$

The bias error of the heat flux is determined as the RSS of the errors associated with heater plate area A_{hp} and power to the heater plate q_e:

$$\frac{B(q'')}{q''} = \left[\left(\frac{B(A_{hp})}{A_{hp}} \right)^2 + \left(\frac{B(VI)}{VI} \right)^2 \right]^{1/2} \tag{6.26}$$

For the conservative case of T_m = 200°C and ΔT = 10 K, the bias error of the heat flux is ±2.0803 %

6.8 Measurement of Thermal Conductivity

The thermal conductivity is determined by the Fourier's law:

$$\lambda = q'' \frac{H}{\Delta T} \tag{6.26}$$

The bias error of the thermal conductivity λ is determined as the RSS of the errors associated with heat flux q'', effective thickness H, of the specimen, and ΔT across the specimen as:

$$\frac{B(\lambda)}{\lambda} = \left[\left(\frac{B(q'')}{q''} \right)^2 + \left(\frac{B(H)}{H} \right)^2 + \left(\frac{B(\Delta T)}{\Delta T} \right)^2 \right]^{1/2} \tag{6.27}$$

For the conservative case of T_m = 200°C, with ΔT = 10K, the bias errors of the thermal conductivity is ± 2.236 %.

CHAPTER 7

MEASUREMENT PROCEDURES

7.1 Specimen Preparations and Start-up

An accurate measure of the weight and moisture content for the soil sample is required before the start of an experimental run. The weight of the empty specimen container with 149.42 mm diameter was determined before it was filled with soil and compacted to the desired density. The specimen container is 20.83 mm deep and is covered by an overlapping lid. The entire container is made from 0.23 mm thick electroplated mild steel. The soil was loosely poured into the container then compacted with a known weight for twenty-four hours, this was repeated until the container was filled with compact soil. A known mass of water was then added to the soil corresponding to the required moisture content. The container was then covered with the lid, sealed with epoxy and placed in a constant temperature environment for forty-eight hours, allowing the moisture to be evenly distributed.

The specimen was first placed between the plates, clamped and leveled. The frame was locked in the desired angular position. The plates were aligned in the horizontal position with heating from top to bottom as the default orientation to minimize the occurrence of any convection in the experiment. The starting temperature was entered and the circulating baths were powered on through the computer program; also, all other equipment was started and allowed sufficient time to be warmed up before running an experiment. The plates, hoses and baths were inspected and checked for leaks.

7.2 Experiment Procedures

A PCI card, Blue-heat from Connect Tech Inc., was inserted in the computer used for the control of the GHP apparatus. This card provides four additional serial communication ports used to connect the circulating baths, the programmable power supply and the data acquisition unit. The computer program (see Appendix C for more details) automates the operation of the experiments after all the equipment is turned on and warmed up. Once the apparatus is inspected and passed, a set of experiments can now be performed.

The hot and cold plate temperatures were allowed to stabilize, via the circulating baths at different temperature settings. During the time allowed for the plate temperatures to stabilize, the electrical power output to the heater plate was turned on and heater plate temperature was allowed an hour to stabilize. The electrical power to the heater plate is balanced in such a way that the heater plate temperature matches the temperature of the hot plate using a feedback loop. The *emf* produced by the HFM, as a result of the temperature difference between the heater plate and hot plate, is used as the sensor for the feedback loop. The process to match the heater plate and hot plate temperatures employs a "high-low" control method.

This method operates on the principle of continuously narrowing the range in which the required power setting lies. The high and low power levels were applied alternatively in such a way that, as soon as the *emf* of the HFM indicates that the heater plate temperature (T_{htr}) is below the hot plate temperature (T_h), the power is increased to a higher level or reduced to a lower level if T_{htr} is above T_h. This process continues for thirteen such adjustments, while the total amount of time spent, Δt, when the power was at either a high or low level was recorded. An average power setting, P'_{est}, required to maintain T_{htr} equal to T_h could then be calculated using Eq. (7.1), for a cycle of thirteen adjustments with the power P' at either a high or low value.

$$P'_{est} = \frac{1}{T}\sum_{i=2}^{13} P'_i \Delta t_i \qquad (7.1)$$

where

$$T = \sum_{i=2}^{13} \Delta t_i \qquad (7.2)$$

The first time period, Δt_1, was neglected because it was usually an unrepresentative amount of time required for the power supply to initially adjust the heater plate from an arbitrary starting condition. The new value of P'_{est} was then used as the best estimate for the power setting of the next cycle. The range between the high and low power levels was then reduced by ½, with its centre at P'_{est}. The cycle was repeated until the range had converged to the power control resolution of about 0.0028 volts. The last value of P'_{est} was then used as the "correct" value of the power setting. The entire process to achieve isothermal conditions between T_{htr} and T_h with the "correct" P'_{est} could take a long time.

Once the "correct" P'_{est} was found, data acquisition started right away, with no need for an additional waiting period. This is so because it had already taken a long time to obtain the "correct" P'_{est} and the last cycle of one power-control resolution above and below the "correct" P'_{est} continued during the data acquisition process to ensue that the "true" P'_{est} could be obtained by Eq. (7.1), which might lie within the power-control resolution. A total of 512 measurements of the following quantities were taken when steady state conditions were achieved:

a. *emf* from the HFM,

b. heater plate power,

c. temperatures of the hot plates and

d. temperature difference between the hot and cold plates.

The variations in each measurement were recorded to determine the precision error associated with each. With these data, the thermal conductivity, along with the corresponding errors, could be calculated by the computer.

The system would repeat the above procedure for the next temperature setting until the final one was reached.

CHAPTER 8

CONCLUSIONS AND RECOMMENDATIONS

8.1 Conclusions

There is a growing demand for accurate experimentally-derived soil thermal conductivity measurements to enhance theoretical models and simulation software, as a result of the increased importance of environmental issues, such as high voltage transmission cables being placed underground, as opposed to the present practice. Also, energy conservation benefits from underground industrial installations have placed renewed interest in soil thermal properties. It is for these reasons that this study was undertaken to provide a means of obtaining accurate soil thermal conductivity data.

A guarded hot plate apparatus was designed and constructed for high temperature applications. Steady state soil thermal conductivity measurement can be derived for temperatures ranging from 20°C to 200°C from this apparatus. The derived thermal conductivity data for soil will have a bias error around ±2% of the mean values, based on the error analysis done in Chapter 6.

8.2 Recommendations

The experiments with this apparatus should be continued and concluded with accurate thermal conductivity data for various soils. The apparatus have the flexibility for the plates to be tilted, thus allowing experiments involving convection with little or no modification required. Although the main application of the GHP apparatus is to measure thermal conductivity of soils, it is also capable of performing thermal conductivity measurements of other materials.

APPENDIX A

CALIBRATION PROCEDURES

A.1 Introduction

This appendix gives a description of the calibration processes for the various sensor and measuring devices used throughout the experiment. A brief description of the need for calibration will be given, as well as the procedure used for the following temperature sensors.

- Baths' internal and external RTDs
- Plate embedded RTDs
- HFM

A.2 Circulating Bath Internal and External RTDs

The calibration procedure for the Neslab RTE series circulating baths' internal RTDs, as outlined in the flow diagram of Figure A-1, provided by the manufacturer of the units, Thermo Electron Corp., was followed to ensure the accuracy of the bath temperatures. Using the Azonix PRT, with a four wire circuit, attached to the Daytronic System 10 Unit, the bath was run at the low-end temperature of 0°C and allowed to stabilize for about 20 minutes, ensuring uniform temperature distribution throughout the reservoir and plates. The procedure was followed, for the low-end calibration, to set

the bath temperature to match that of the PRT's output converted to temperature. The above process was repeated for a suitable high-end calibration point and changes saved to complete the calibration process.

The external RTDs of the circulating baths were attached to the back surfaces of the main plates near the plate's centers and epoxied along isotherms. The circulating baths can be operated to monitor fluid temperature and match a plate temperature set-point via the external RTDs. The external RTDs were calibrated against the temperature output of the Azonix PRT, which was housed in an aluminum block clamped between the plates. The bath was run at the high-end temperature of 200°C and allowed to stabilize, and then the procedure was followed for the high-end calibration, outlined in the flow diagram of Figure A-2. The process was then repeated for a suitable low-end calibration point, and changes saved to complete the calibration process.

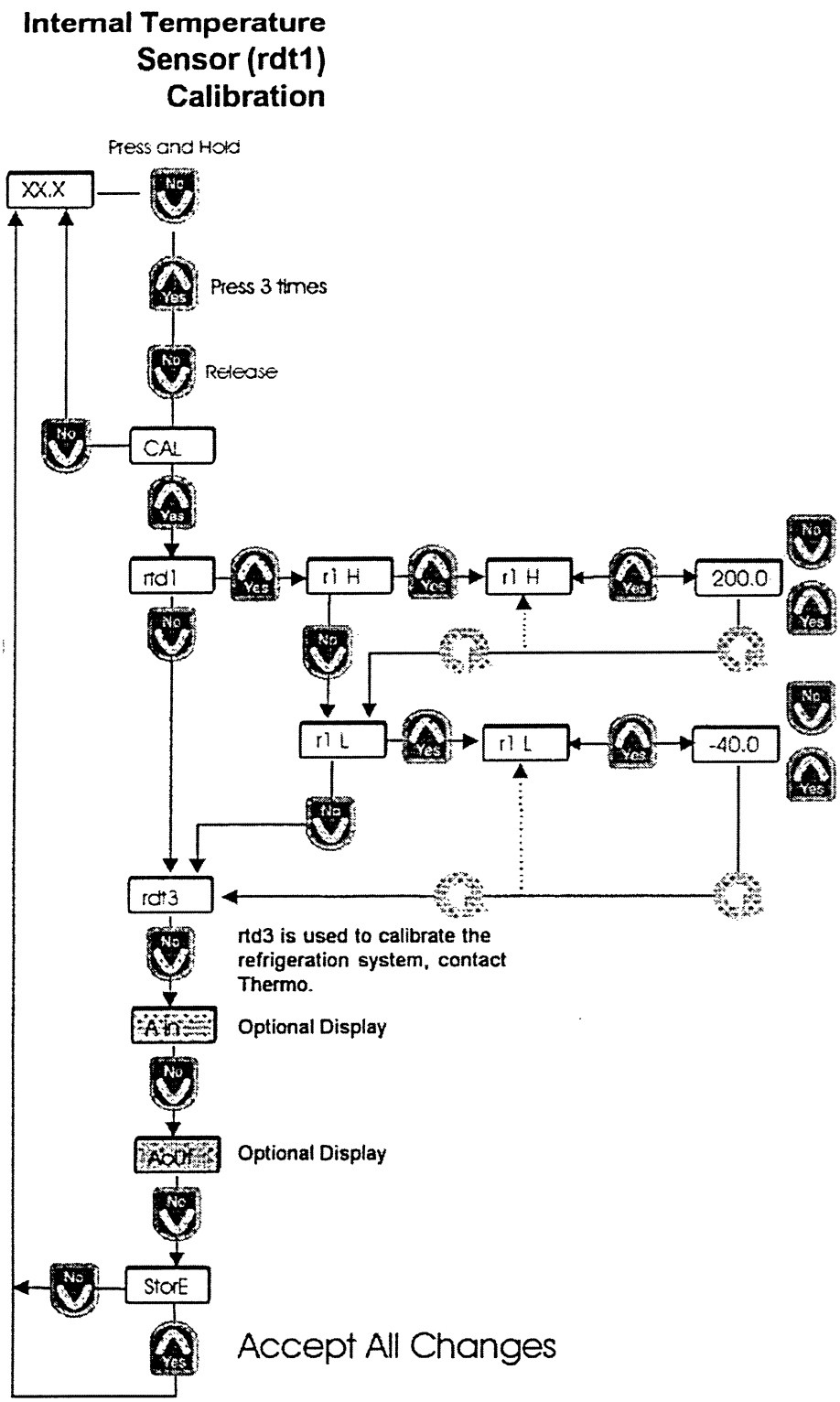

Figure A-1 Calibration Flow diagram – Internal RTDs.

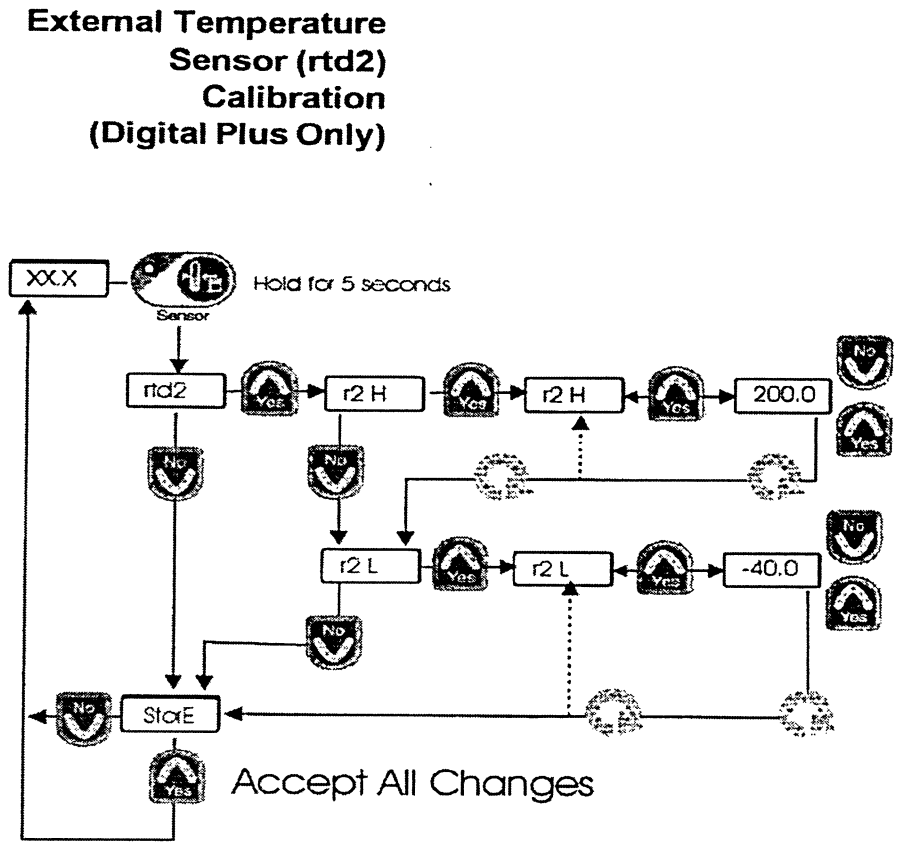

Figure A-2 Calibration Flow diagram – External RTDs.

A.3 Plate Embedded RTDs

After calibration of the baths' internal RTDs, the apparatus was insulated using a 50 mm glass fiber blanket to house the plates. During the *in situ* calibration of the RTDs, a 25 × 76 × 50 mm aluminum block sandwiched between the plates was used to host the PRT. The hot and cold plates with the RTDs attached, as outlined in Chapter 3, was cycled over the temperature range of interest (0°C to 200°C) at 5°C intervals, with both plates at the same temperature. Four-wire circuits measured the voltage outputs from the PRT and RTDs; the same setup was used later in the experiments. These data were collected by the data acquisition sub-routine written in the automation program. At any one of the temperature settings of the circulating baths, the program would wait until the system is steady,

identified by the voltage output of the PRT being constant (variation < 25 μV or 0.013 K) in time over a period of 10 minutes. Then, measurements were made 256 times over a period of about fifteen minutes. The voltage output of the PRT read into the program was converted to temperature and that of the RTDs was converted to resistances. Using least squares analysis, fourth order polynomial fit were obtained between the PRTs' temperatures and the RTDs' resistances. These equations, derived for temperature intervals of 50 degrees, are then used in the computer program to produce the plate surface temperature. The maximum standard fit error between the two RTDs was 0.01 K. From an analysis of error in these results, it was concluded that the error in temperature (see Chapter 6) caused by the use of the fitted equations was ±0.0283 K, including the measurement error of the Daytronic System 10 unit.

A.4 The Heat Flux Meter

The proportional constant α of the heat flux meter can be determined *in situ* after assembly of the entire apparatus. Since it is not very important to have an accurate value of α, its value was obtained for each set of experiments at a fixed T_m and δT, using the following calibration procedure.

1. Between the plates is clamped an insulating material of known thermal conductivity as a reference. This establishes a basis for calculating the proportional constant α by a comparative method.

2. To obtain the value of α at conditions as close to the experimental conditions as possible, the setting of the programmable power supply, which makes the temperature T_{htr} of the heater plate equal to the temperature T_h of the hot plate, should first be approximately obtained. Once that particular setting is known, settings on each side of it can be set, allowing the temperature of the heater plate to be varied

from slightly higher to slightly lower than T_h. Usually, seven settings were enough to make a good curve fit to obtain the proportional constant α. Over these settings, the temperature difference between T_{htr} and T_h varied normally between ±0.2 K.

3. At each increment of the setting of the programmable power supplied to the heater plate, the *emf* of the heat flux meter **e**, the electrical power to the heater plate q_e, the temperature difference between the cold plate and the hot plate ΔT, and the temperature difference between the heater plate and the hot plate δT are measured and averaged over 512 data points for a time span of about 30 minutes, under steady state conditions. A steady state is considered when the fluctuation of the *emf* **e** is less than 25μV per minute.

4. To obtain the proportionality constant α, a steady state heat balance of the heater plate gives

$$q_e = q_b + q_c \qquad \textbf{(A.1)}$$

The subscripts ***b*** and ***c*** represent the back and the front surface of the heater plate, respectively.

The heat flow rates are given by

$$q_b = h_b A_b (T_{htr} - T_h)$$

and

$$q_c = \lambda A_c (T_{htr} - T_c)/\Delta x$$

Therefore Eq. (A.1) becomes

$$q_e = h_b A_b (T_{htr} - T_h) + \lambda A_c (T_{htr} - T_c)/\Delta x \qquad \textbf{(A.2)}$$

where h is the heat transfer coefficient, λ and Δx are the reference material thermal conductivity and thickness, respectively, and A is the surface area of the heater plate.

Eq. (A.2) is useful if T_{htr}, T_c and T_h are measured and known. In order to minimize the error associated with the reference material thermal conductivity, T_c is set equal to T_h; thus q_c will be very small. With the data set obtained from step 2, h_bA_b can be obtained as the slope of the graph of $q_e - \lambda A_c (T_{htr} - T_c)/\Delta x$ vs $(T_{htr} - T_c)$. Once h_bA_b is determined, the heat transfer from the heater plate to the hot plate can be evaluated as

$$q_b = h_bA_b(T_{htr} - T_h).$$

Another method is to utilize the heat flux meter, such that Eq. (A.1) becomes

$$q_e - \lambda A_c (T_{htr} - T_c)/\Delta x = \alpha e \qquad \textbf{(A.3)}$$

The calibration constant α can be obtained as the slope of the graph of $q_e - \lambda A_c (T_{htr} - T_c)/\Delta x$ vs. e. Once α is determined, the heat transfer from the heater plate to the hot plate can be evaluated as

$$q_b = \alpha e$$

The calibration constant α was determined by the least squares method to within ±0.5% by the procedure described.

APPENDIX B

CONDUCTION ERROR OF THERMOCOUPLE WIRES EMBEDDED IN A PLATE

B.1 Introduction

An analysis is under taken to evaluate the effect of embedded thermocouple wires on temperature measurements for the heated plates. Heat loss by conduction through thermocouple wires can cause considerable errors in temperature measurements. The minimum length of wire needed to be affixed on an isotherm of the surface, to minimize conduction losses as well as the overall uncertainty in temperature measurement, is determined in this analysis.

Figure B-1 shows a thermocouple embedded a depth l into a medium with temperature T_{md}. The lead wire of the thermocouple with perimeter P, cross-sectional area A and thermal conductivity λ is affixed on the surface of the medium over a length L before being extended infinitely long into the ambience at temperature T_a. The conduction loss through the entire length of the wire is evaluated by the following equations as outlined in Leong [13],

(i) In the hole in the medium:

$$\frac{\partial^2 T}{\partial x^2} - \omega_{md}^2 (T - T_{md}) = 0 \qquad \textbf{(B.1)}$$

(ii) On the surface of the medium:

$$\frac{\partial^2 T}{\partial x_1^2} - \omega_{sa}^2 (1-\xi)(T - T_a) - \omega_{smd}^2 \xi (T - T_{md}) = 0 \qquad \textbf{(B.2)}$$

(iii) In the ambience:

$$\frac{\partial^2 T}{\partial x_2^2} - \omega_a^2 (T - T_a) = 0 \qquad \textbf{(B.3)}$$

where

$$\omega^2 = \frac{hP}{\lambda A} = \frac{4h}{\lambda D}$$

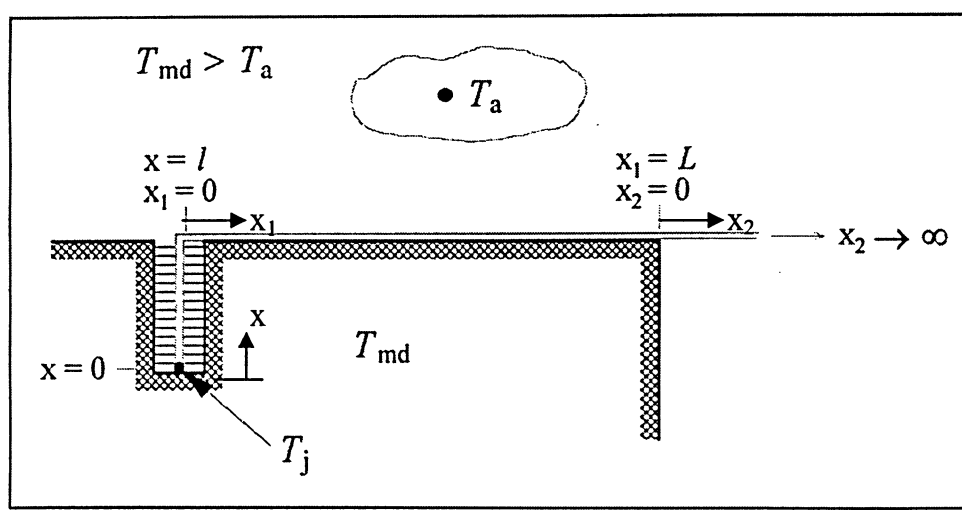

Figure B-1 Embedded thermocouple wire (Leong [13]).

given for round wires, h is the heat transfer coefficient pertaining to the location of the wire and ξ is the fraction of wire perimeter that is affixed on the surface of the medium. As shown in Figure B.1, x represents the embedded portion of wire from the depth of the hole to the surface of the medium; wire affixed on the surface of the medium is represented by x_1, from the hole to the edge of the medium; and wire extending into the ambient from the edge of the medium is represented by x_2.

The following six boundary conditions must be satisfied:

(i) Heat flux at the junction (thermocouple) is negligible:

$$\left(\frac{dT}{dx}\right)_{x=0} = 0$$

(ii) Temperature is continuous:

$$T_{x=l} = T_{x_1=0},\ T_{x_1=L} = T_{x_2=0},$$

(iii) Heat flux is continuous:

$$\left(\frac{dT}{dx}\right)_{x=l} = \left(\frac{dT}{dx_1}\right)_{x_1=0},\ \left(\frac{dT}{dx_1}\right)_{x_1=L} = \left(\frac{dT}{dx_2}\right)_{x_2=0}$$

(iv) As $x_2 \rightarrow \infty$, $T \rightarrow T_a$.

Solving Eqs.(B.1), (B.2) and (B.3) with the boundary conditions given, the measurement error caused by the conduction loss through the wire is obtained as

$$T_{md} - T_j = \frac{\left[e^{\omega_s L} + \left(\frac{\omega_s}{\omega_a} - 1\right)\sinh \omega_s L\right](T_{md} - T_{sma}) - (T_a - T_{sma})}{e^{\omega_s L}\beta + \left(\frac{\omega_s}{\omega_a} - 1\right)\gamma} \qquad \textbf{(B.4)}$$

where T_j is the temperature at the thermocouple junction, i.e., $T_j = T(x = 0)$. If the wire is extended to the ambience directly without being affixed on the surface of the medium, i.e. $L = 0$, then Eq. (B.4) simplifies to

$$(T_{md} - T_j)_{max} = \frac{T_{md} - T_a}{\cosh \omega_{md} l + \frac{\omega_{md}}{\omega_a} \sinh \omega_{md} l} \qquad \textbf{(B.5)}$$

which will result in the maximum error. If, however, the wire is affixed an infinite length on the surface of the medium, i.e., $L \rightarrow \infty$ and $\omega_a = 0$, then Eq. (B.4) becomes

$$(T_{md} - T_j)_{min} = \frac{T_{md} - T_{sma}}{\cosh \omega_{md} l + \frac{\omega_{md}}{\omega_s} \sinh \omega_{md} l} \qquad \textbf{(B.6)}$$

which is the minimum error caused by conduction losses through the wire.

Since affixing the wire an infinite distance ($L \rightarrow \infty$) on the surface of the medium is impractical, the minimum error can only be closely achieved for a suitable finite length L.

B.2 Calculations of Error

With copper having thermal conductivity $\lambda = 393$ W/mK, which is much larger than that of constantan, it is responsible for most of the conduction losses. Therefore, only the copper wire is considered in the evaluation to follow. Experimental conditions of $T_{md} = 200°C$ and $T_a = 25°C$ are applied throughout the evaluation to achieve the most conservative results. A summary of the

parameters used in the evaluation are given in Table B.1. These values are derived from correlations and data from Incropera and DeWitt [24] and Holman [25] to be as realistic as possible. All calculations were done using Waterloo_Maple 7.

Table B.1 Values of heat transfer parameters for thermocouple in a hole 3.18 mm diameter and 17.46 mm depth, filled with epoxy at the hot plate.

	Location of wire		
	In the hole	On the surface	In the ambience
h_{md} (W/m^2.K)	4076.5		
ω_{md} (m^{-1})	385.4		
h_{sa} (W/m^2.K)		101.3	
h_{smd} (W/m^2.K)		8456.1	
ω_{sa} (m^{-1})		60.7	
ω_{smd} (m^{-1})		555.0	
ξ		0.1	
ω_s (m^{-1})		184.7	
h_a (W/m^2.K)			87.9
ω_a (m^{-1})			56.6

Values are evaluated based on wire diameter D = 127 μm (bare wire), and D_o = 297 μm (with Teflon)

Using the data in Table B.1 for 36-gauge Teflon insulated copper wire, for the hot plate the maximum and minimum errors are 0.05056 K and 0.0125 K, respectively. However, since the experimental model is covered with 50-mm thick fiberglass insulation, h_{sa} reduces significantly to 12.21 W/m^{2}K; correspondingly, ω_{sa} = 21.1 m^{-1} and ω_s = 176.7 m^{-1}. The minimum error decreases to only 0.0016 K.

For the cold plate, the depth of the hole is decreased to 11.11 mm. The maximum and minimum

errors are 0.548 K and 0.13401 K, respectively, for 36-gauge Teflon insulated copper wire. With a 50-mm fiberglass insulation, the minimum error reduces to 0.018 K.

76.2 μm (40-gauge) Teflon insulated wire was used for the heater plate thermocouple. This was inserted in a hole 1.59 mm in diameter by 2.6 mm in depth filled with epoxy. For the heater plate, ω_{md} was found to be 1373.3 m^{-1}. Between the heater plate and the hot plate, there is a small air gap, about 3 mm in width and a small temperature difference; therefore, a heat transfer coefficient of 52.5 W/m^2K, including the effects of Teflon insulation and radiation, is used as h_{sa}; correspondingly, ω_{sa} = 83.8 m^{-1}. The heat transfer coefficients h_{smd} and h_a increase to 2780.4 W/m^2K and 210.9 W/m^2K, respectively, as a result of the decrease in wire diameter; correspondingly, ω_{smd} = 609.4 m^{-1} and ω_s = 208.5 m^{-1}; hence, ω_{sa} = 167.8 m^{-1}. Therefore, the maximum and minimum errors for the heater plate are obtained as 0.006 K and 0.0011 K.

The above calculations showed that increasing either the depth of the hole, *l*, or the length of the wire, L, could reduce the conduction error. A minimum length *L* of 80 mm affixed on the surface is required to minimize the error to within 0.01 K. A layer of insulation covering the wire on the surface also has a significant effect in reducing the conduction error.

APPENDIX C

GHP APPARATUS AUTOMATION AND CONTROL

C.1 Introduction

A computer program was written in Microsoft Visual Basic 6.0 to automate the experiments of the GHP apparatus and coordinate the supporting equipment. This program was necessary to control the equipment operation because of the lengthy run-time expected to achieve steady state conditions. This program monitors critical parameters such as *emf* output, plate temperature and power supply, in an effort to maintain the safe operation of the GHP apparatus. Real-time feedback is provided to the operator and milestone achievements are recorded for future reference. The program also has the capability to determine steady state for each plate temperature set-point and initiates data acquisition of vital data needed in the calculation of the thermal conductivity and relevant errors of the specimen under investigation.

The flow path illustrated in Figure C-1 shows the execution process of the computer program. The actual operation of which is explained with more detail in Chapter 7. The various stages of the process are controlled by sub-routines and functions in different combinations. An on-screen display, shown in Figure C-2, is used to indicate the operation status and request an operator's input at various check points.

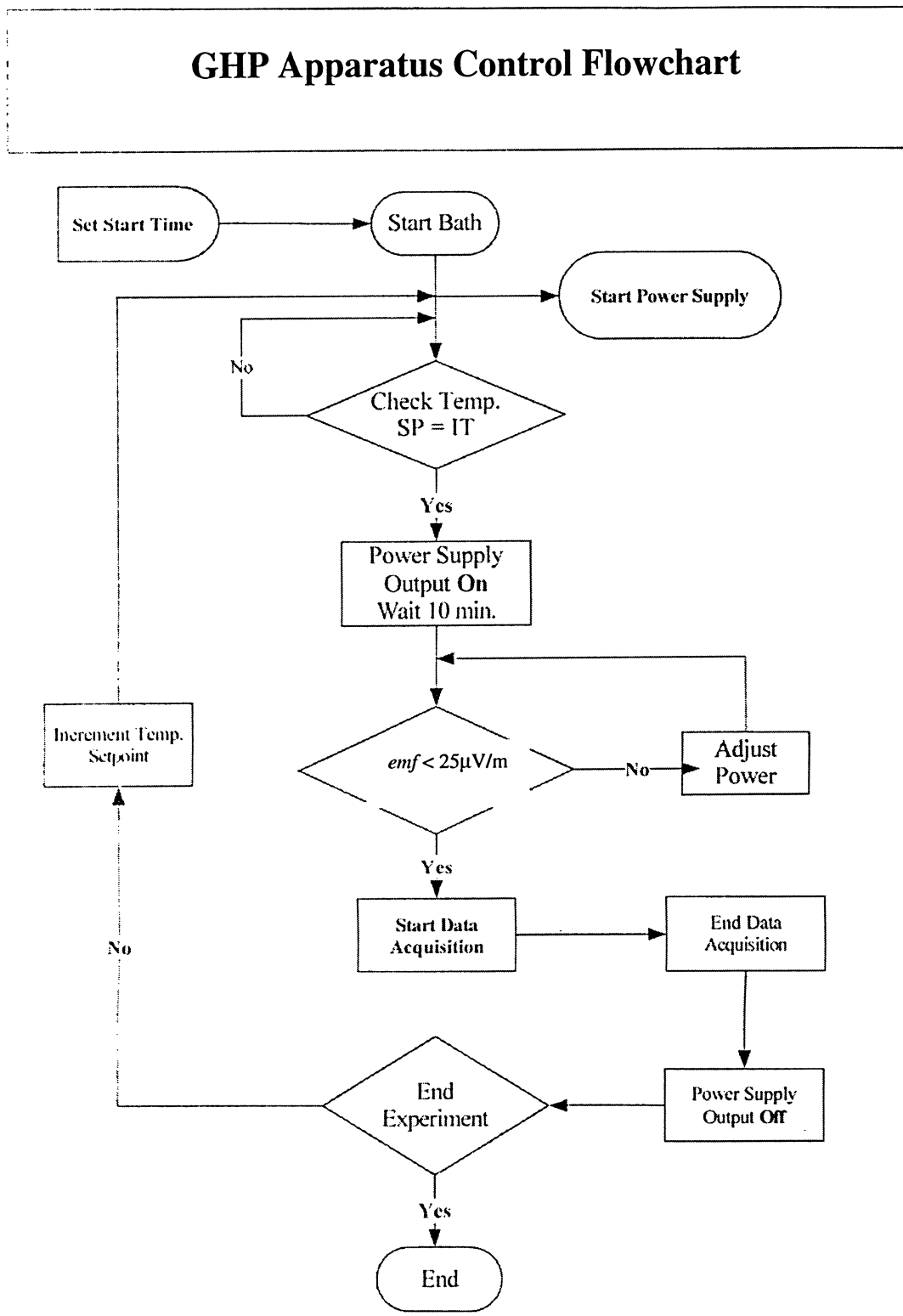

Figure C-1 GHP apparatus control flowchart

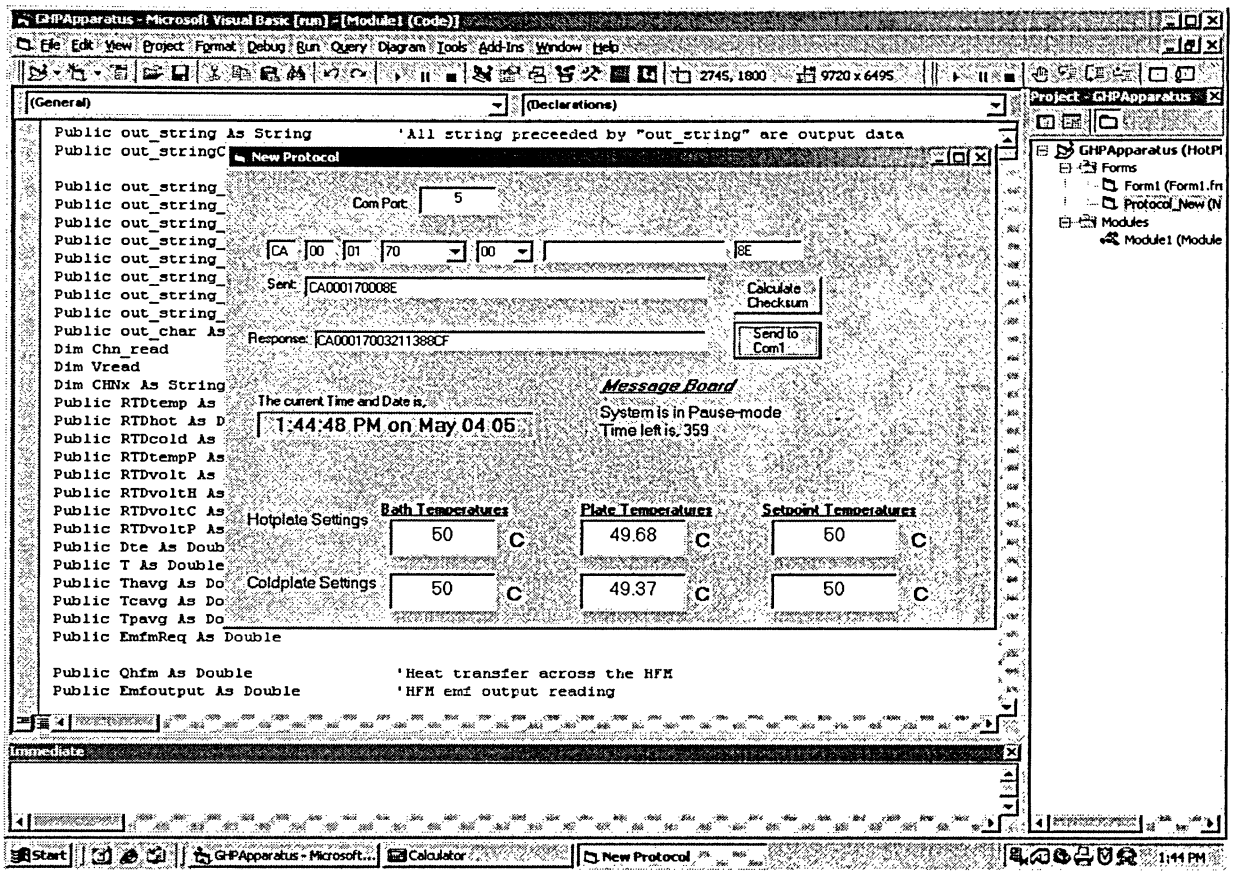

Figure C-2 A snapshot of the on screen display of Hot Plate-Control

APPENDIX D

ENGINEERING DRAWING OF THE GHP APPARATUS

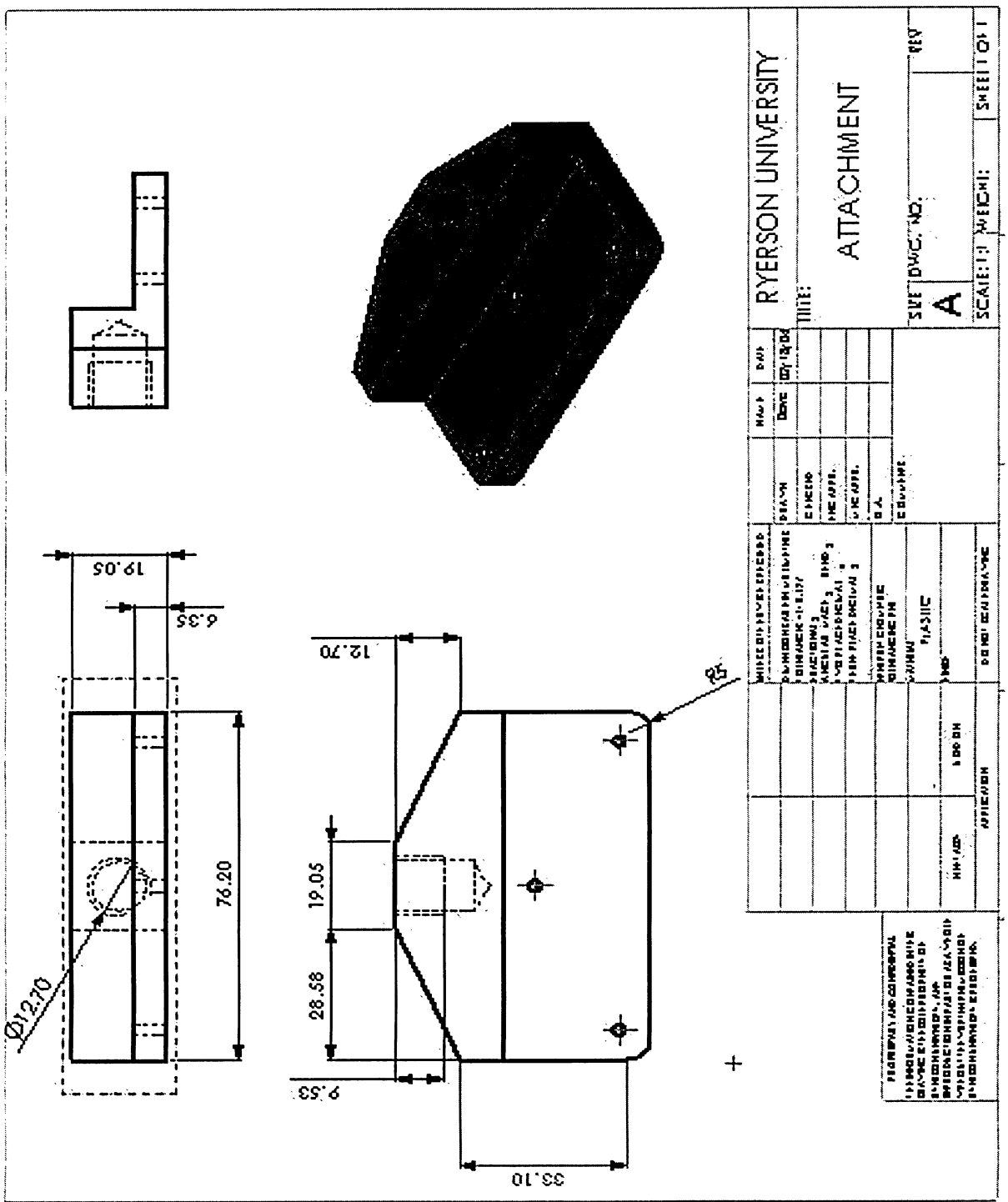

REVISIONS				
ZONE	REV.	DESCRIPTION	DATE	APPROVED

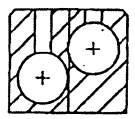

A-A

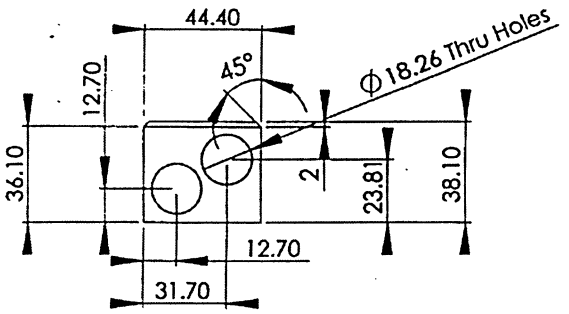

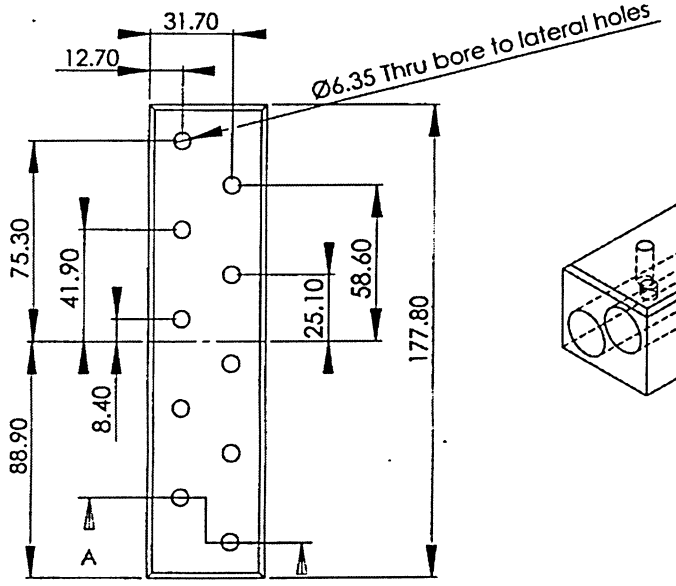

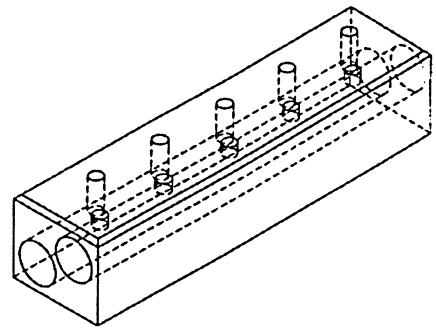

		DIMENSIONS ARE IN MILLIMETERS TOLERANCES: +/- 0.127 FRACTIONAL ± ANGULAR: MACH ± BEND ± TWO PLACE DECIMAL ±		NAME	DATE	RYERSON UNIVERSITY
			DRAWN	DAVE	12/01/04	
			CHECKED			
			ENG APPR.			
			MFG APPR.			
			Q.A.			Req. no. off: 2
		MATERIAL COPPER	COMMENTS:			
NEXT ASSY	USED ON	FINISH				
APPLICATION		DO NOT SCALE DRAWING				SIZE A DWG NO. Header Block REV. 2
						SCALE 1:2 WEIGHT SHEET 1

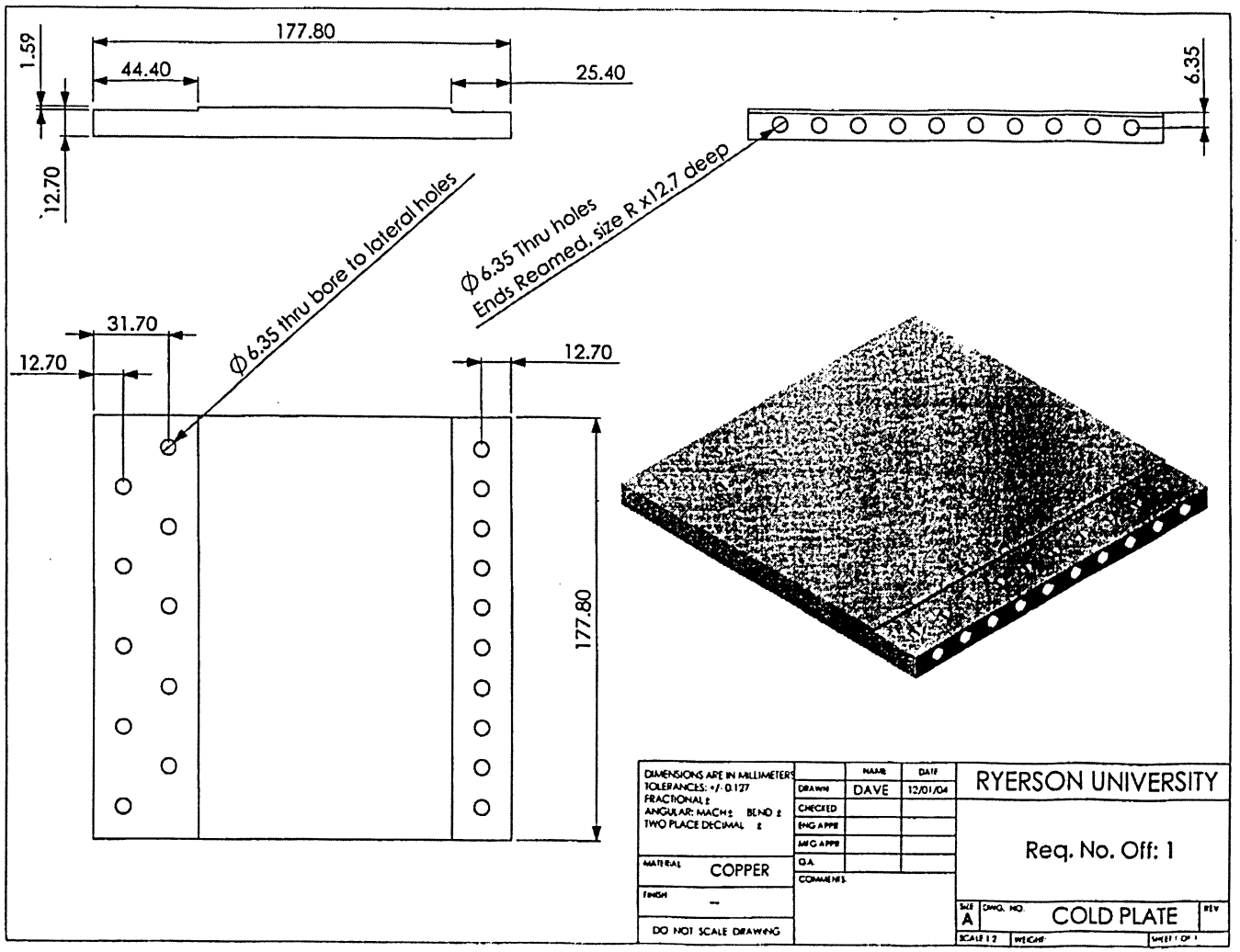
177.80
44.40
25.40
1.59
12.70
6.35
Ø6.35 thru bore to lateral holes
Ø6.35 Thru holes
Ends Reamed, size R x12.7 deep
31.70
12.70
12.70
177.80
DIMENSIONS ARE IN MILLIMETERS
TOLERANCES: +/- 0.127
FRACTIONAL ±
ANGULAR: MACH ± BEND ±
TWO PLACE DECIMAL ±
MATERIAL COPPER
FINISH —
DO NOT SCALE DRAWING
NAME DATE
DRAWN DAVE 12/01/04
CHECKED
ENG APPR
MFG APPR
Q.A.
COMMENTS:
RYERSON UNIVERSITY
Req. No. Off: 1
SIZE A
DWG. NO. COLD PLATE
REV
SCALE 1:2
WEIGHT:
SHEET 1 OF 1

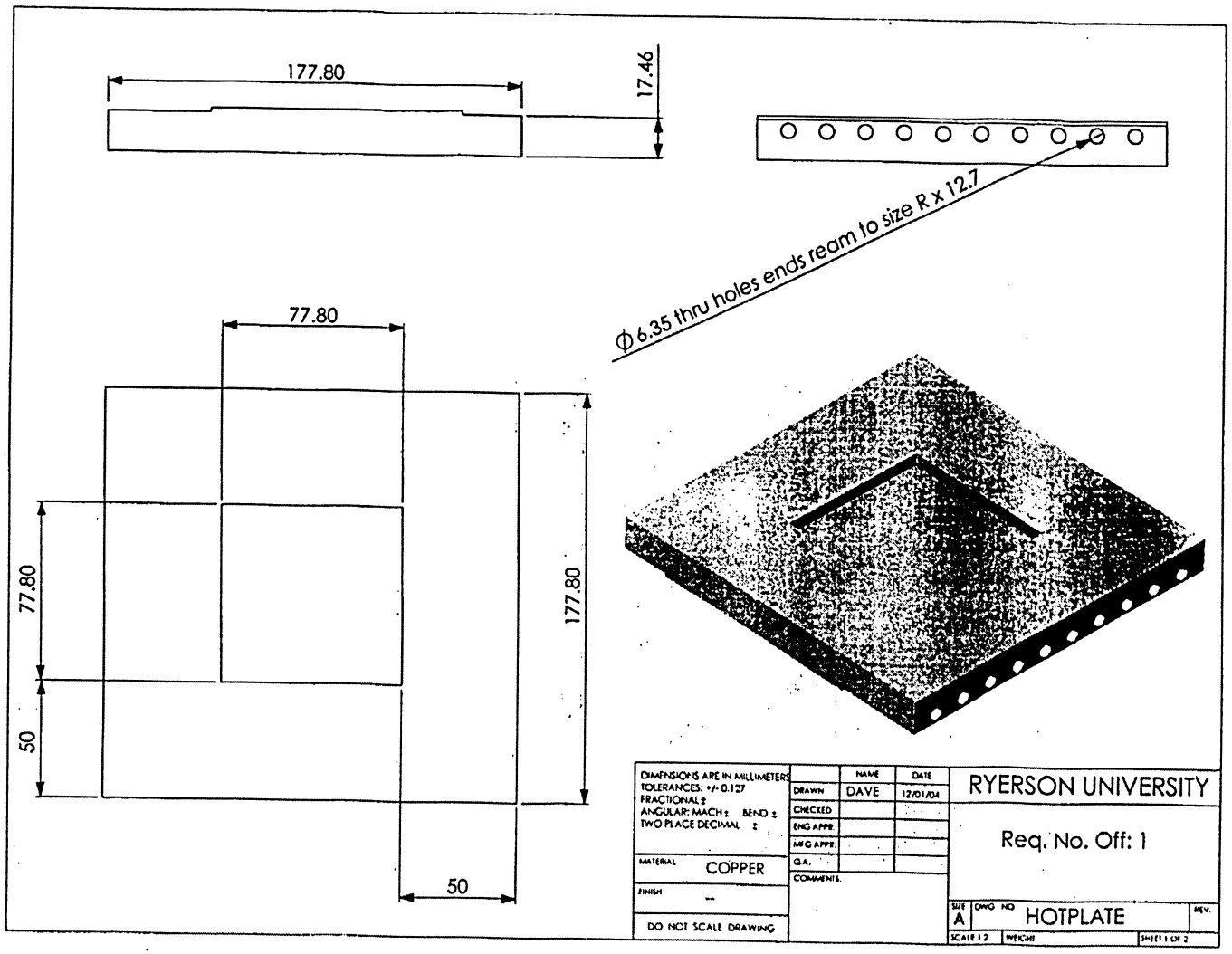
177.80
17.46
Φ6.35 thru holes ends ream to size R x 12.7
77.80
77.80
177.80
50
50
DIMENSIONS ARE IN MILLIMETERS
TOLERANCES: +/- 0.127
FRACTIONAL ±
ANGULAR: MACH ± BEND ±
TWO PLACE DECIMAL ±
MATERIAL COPPER
FINISH —
DO NOT SCALE DRAWING
NAME DATE
DRAWN DAVE 12/01/04
CHECKED
ENG APPR.
MFG APPR.
Q.A.
COMMENTS:
RYERSON UNIVERSITY
Req. No. Off: 1
SIZE A
DWG NO HOTPLATE
REV.
SCALE 1:2
WEIGHT
SHEET 1 OF 2

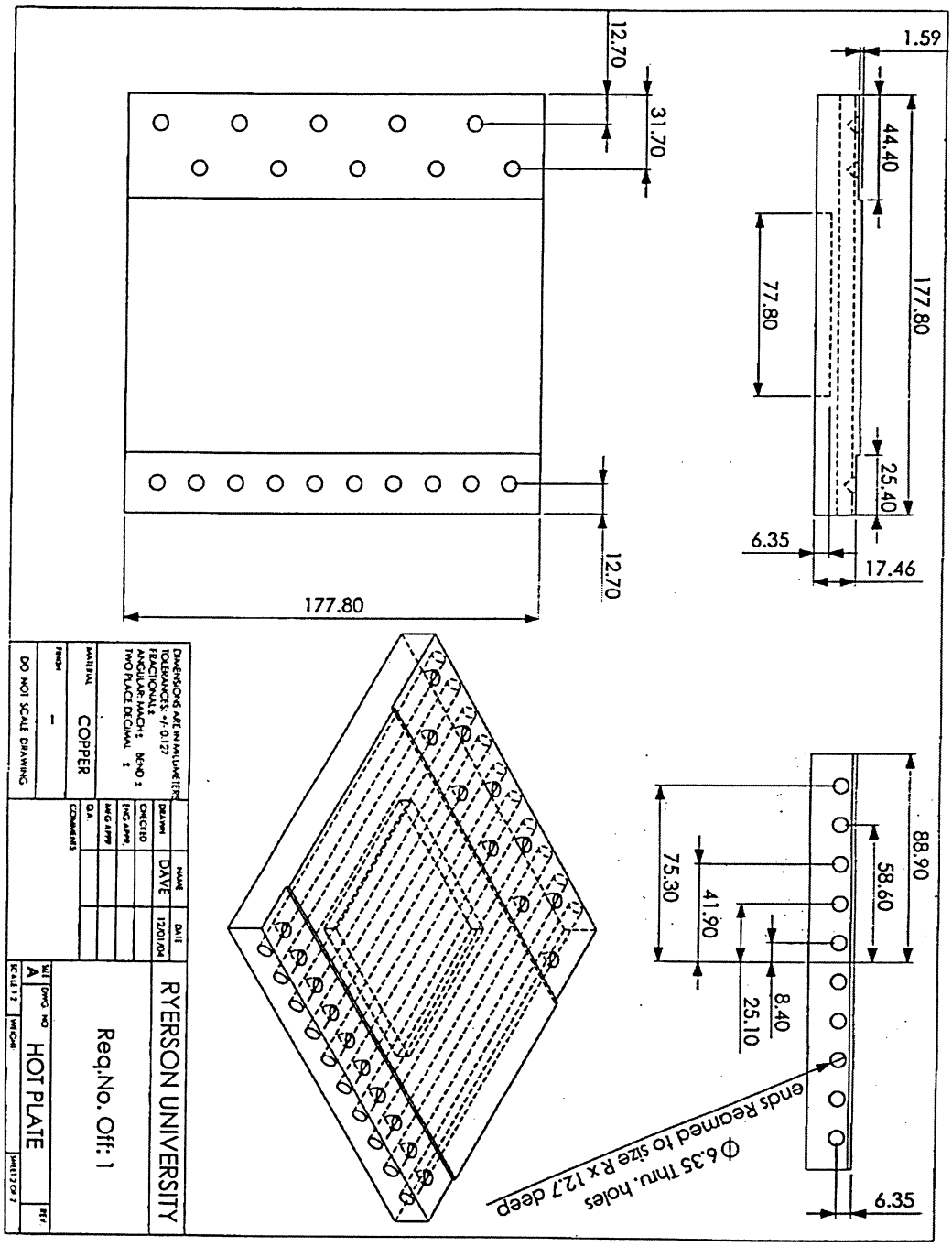
1.59
44.40
177.80
77.80
25.40
6.35
17.46
12.70
31.70
12.70
177.80
88.90
58.60
75.30
41.90
25.10
8.40
Ø 6.35 Thru. holes
ends Reamed to size R x 12.7 deep
6.35
DIMENSIONS ARE IN MILLIMETERS
TOLERANCES: +/- 0.127
FRACTIONALS
ANGULAR: MACH: BEND: ±
TWO PLACE DECIMAL ±
MATERIAL COPPER
FINISH —
DO NOT SCALE DRAWING
NAME
DATE
DRAWN DAVE 12/01/04
CHECKED
ENG APPR.
MFG APPR.
Q.A.
COMMENTS
RYERSON UNIVERSITY
Req.No. Off: 1
SIZE A
DWG NO HOT PLATE
REV
SCALE 1:2
WEIGHT
SHEET 1 OF 1

REFERENCES

[1]. Dey, C., Read, A., Collins, R. and Brunotte, M.,, *A Guarded Cold Plate apparatus for absolute measurement of heat flow*, Int. Journal of Heat and Mass Transfer 1998, Vol. 41, pg. 3099 – 3108

[2]. Gori, F. and Corasaniti, S., *Theoretical Predictions of the Soil Thermal Conductivity at Moderately High Temperature,* Journal of Heat Transfer 2002, Vol. 124, pg. 1001 – 1008

[3]. Tarnawski, V. and Leong, W., *Thermal Conductivity of Soil at Very Low Moisture Content and Moderate Temperatures,* Transport in Porous Media 2000, Vol. 41, pg. 137 –147

[4]. Tarnawski, V. and Gori, F., *Enhancement of the cubic cell soil thermal conductivity model,* Int. Journal of Energy Research 2002, Vol. 26, pg. 143 – 157

[5]. Shiozawa, S. and Campbell, G., *Soil Thermal Conductivity,* Remote Sensing Review 1990, Vol. 5, pg. 301 – 310

[6]. Sepaskhah, A. and Boersma, L., *Thermal Conductivity of Soils as a Function of Temperature and Water Content,* Soil Science Society 1979, Vol. 43, pg. 439 – 444

[7]. Campbell, G. Jungbauer (Jr.), J., Bidlake, W. and Hungerford, R., *Predicting the Effect of Temperature on Soil Thermal Conductivity,* Soil Science 1994, Vol. 158, No.5, pg. 307 – 313

[8]. Hiraiwa,Y. and Kasubuschi,T., *Temperature dependence of thermal conductivity of soils over a wide range of temperature (5 – 75 °C),* European Journal of Soil Science 2000, Vol. 51, pg. 211 – 218

[9]. Black, W., Bush, R. and Martin Jr., M., *Soil Thermal Properties and Their Effect on Thermal Stability and the Rating of Underground Power Cable*, 7th IEEE/PES Transmission and Distribution Conference and Exposition 1979, pg. 275 – 280

[10]. Salmon, D., *Thermal Conductivity of Insulations using Guarded Hot Plates, Including Recent Developments and Sources of Reference Materials,* Measurement Science and Tech. 2001, Vol. 12, pg. R89 – R98

[11]. Zarr, Robert R., *A History of Testing Heat Insulators at the National Institute of Standards and Technology,* ASHRAE Transactions 2001, V. 107, Pt. 2

[12]. Hollands, K. G., *Direct Measurement of Gaseous Natural Convective Heat Fluxes,* Experimental Heat Transfer, Fluid Mechanics and Thermodynamics, Shah *et al.* 1988, Elsevier, New York, pg. 160 – 168

[13]. Leong, W. H., *Benchmark Experiments on Convection Heat Transfer Across a Cubical Cavity,* PhD Thesis 1996, University of Waterloo, Waterloo Ontario Canada

[14]. Beck J.V. and Hurwicz H., *Effect of Thermocouple Cavity on Heat Sink Temperature,* Journal of Heat Transfer 1960, Vol. 82, No. 1, pg. 27 – 36

[15]. Moffat, R. J., *Experimental Methods in Heat Transfer,* Experimental Heat Transfer, Fluid Mechanics and Thermodynamics, Shah et al. 1988, Elsevier New York, pg. 13 – 31

[16]. Bajura, R. A. and Jones, (Jr.) E. H., *Flow Distribution Manifolds,* Journal of Fluid Engineering 1976, pg. 654 – 666

[17]. Datta, A. B. and Majumdar, A. K., *Flow Distribution in Parallel and Reverse Flow Manifolds,* Int. Journal of Heat and Fluid Flow 1980, Vol. 2 No. 4, pg. 253 – 262

[18]. Van der Graaf, F., *Heat Flux Sensors*, Chapter 8 of Volume 4: Thermal Sensors Edited by Ricolfi and Scholz, VCH Verlagsgesellschaft, pg. 297 – 322

[19]. Potter, M., Wiggert, D. and Hondzo, M., *Mechanics of Fluids*, Brooks Cole/Thompson Learning, Pacific Grove 2002

[20]. Graebel, W. P., *Engineering Fluid Mechanics*, Taylor and Francis, New York 2001

[21]. Wang, J. Gao, Z. Gan, G. and Wu, D., *Analytical Solution of Flow Coefficient for a Uniformly Distributed Porous Channel,* Chemical Engineering Journal 2001, Vol. 84, pg. 1 – 6

[22]. Saleh, J. M., *Fluid Flow Handbook*, McGraw-Hill, Toronto 2002

[23]. Burns, G., Scroger, M., and Strouse, G., *Temperature-Electromotive Force Reference Functions and Tables for the Letter-Designated Thermocouple Types Based on the ITS-90*, National Institute of Standards and Technology, Gaithersburg 1993, pg 249 – 280

[24]. Incorpera, F. P. and DeWitt, D. P., *Introduction to Heat Transfer*, John Wiley and Sons 2000, Third Edition

[25]. Holman, J. P., *Heat Transfer*, The McGraw-Hill Companies 1997, Eight Edition

[26]. Clark, S., *NPL Vacuum Guarded Hot-Plate for Measuring Thermal Conductivity and Total Hemispherical Emittance of Insulation Materials,* America Society for Testing and Materials, Insulation Materials: Testing and Applications 2002, Vol. 4, West Conshohocken PA

[27]. Schneider, G. E. Yovanovich, M. M. and Cane, R. L. D., *Thermal Resistance of a Convectively Cooled Plate with Non-uniform Applied Flux,* Journal of Spacecraft Rockets, AIAA 1980, Vol. 17, No. 4, pg. 372 – 376.

[28]. Baver, L. D., *Soil Physics,* John Wiley and Sons, Inc., New York 1956, Third Edition

[29]. Kasubuchi, T. Hiraiwa, Y., *Temperature Dependence of Thermal Conductivity of Soil,* Scientific Registration No. 435, 1997

[30]. Nusier, O., and Abu-Hamdeh, N., *Laboratory Technique to Evaluate Thermal Conductivity for some Soils,* Heat and Mass Transfer 2003, Vol. 39, pg. 119 – 123

[31]. Singh, A. K. Singh, R. and Chaudhary, D. R., *Prediction of Effective Thermal Conductivity of Moist Porous Materials,* Journal of Physics 1990, Vol. 23, pg. 698 – 702

[32]. Becker, R. and Katz, A., *Thermal Conductivity Test of Moist Materials Estimation of Error,* National Building Institute, Isreal, pg. 427 – 432

[33]. *Omega Complete Temperature Measurement Handbook and Encyclopedia*, Vol. 29, Section Z, 1995, pg. 198 – 201

[34]. Filla, B., *A Steady State High-temperature Apparatus for Measuring Thermal Conductivity of Ceramics*, Rev. Science Instrum. 1997, Vol. 68, pg. 28822 – 2829

[35]. Kasubuchi, T. and Hiraiwa, Y., *Temperature Dependence of Thermal Conductivity of Soil*, Scientific Registration No. 435, Symposium No. 1

[36]. De Vries, D., *A Critical Analysis of the Calorimetric Method for Determining the Heat Flux in Soil*, The Eighth International Heat Transfer Conference 1986, San Francisco, California, pg. 473 – 476

[37]. Fujino, J., Honda, T., and Yamashita, H., *Numerical and Experimental Studies on the Measurement of Thermal Conductivity of a Silicone Rubber Plate as a Reference Material*, Heat Transfer—Japanese Research 1997, Vol. 26, No. 7, pg. 435 – 448

[38]. Tarnawski, V., Leong, W., Gori, F., Buchan, G., and Sundberg, J., *Inter-particle Contact Heat Transfer in Soil Systems at Moderate Temperatures*, Int. Journal Energy Res. 2002, Vol. 26, pg.1345 – 1358

[39]. Abu-Hamdeh, N., Khadair, A., and Reeder, R., *A Comparison of Two Methods used to Evaluate Thermal Conductivity for Some Soils*, Int. Journal of Heat and Mass Transfer 2001, Vol. 44, pg. 1073 – 1078

[40]. Adam, E. and Jones, P., *Thermophysical Properties of Stabilised Soil Building Blocks*, Building and Environment 1995, Vol. 30, No. 2, pg. 245 – 253

[41]. Bachmann, J., Horton, R., Ren, T., and van der Ploeg, R., *Comparison of the Thermal Properties of four Wettable and four Water-Repellent Soils,* J. Soil Science Society America Journal 2001, Vol. 65, pg.1675 – 1679

[42]. Hammerschmidt, U., *Guarded Hot Plate (GHP) Method: Uncertainty Assessment*, Int. Journal of Thermophysics 2002, Vol. 23, No. 6 pg. 1551 – 1569

[43]. Willix, J., Lovatt, S. and Amos, N., *Additional Thermal Conductivity Values of Foods Measured by a Guarded Hot Plate*, Journal of Food Engineering 1998, Vol. 37, pg. 159 – 174

[44]. Zarr, R., William, H., Filliben, J. and Flynn, D., *Design Concepts for a New Guarded Hot Plate Apparatus for Use Over Extended Temperature Range*, ASTM Int. Standards, Insulation Material, Testing and Applications 2002, Vol. 4, pg. 98 – 115

[45]. Costamagna, P., Arato, E. Achenbach, E., and Reus, U., *Fluid Dynamic Studies of Fuel Cell Devices: Simulation and Experimental Validation*, Journal of Power Sources 1994, Vol. 52, pg. 243 – 249